

Work Package 2

Theory and modelling

Andrey V. Solov'yov

MBN Research Center, Frankfurt am Main, Germany

www.mbnresearch.com

2nd Year Progress Review Meeting,

EIC-PATHFINDER TECHNO-CLS project 101046458

“Emerging technologies for Crystal-based gamma-ray Light Sources (CLS)”

26 June 2024, on-line

TECHNO-CLS consortium



Istituto Nazionale di Fisica Nucleare

JOHANNES GUTENBERG
UNIVERSITÄT MAINZ



University of
Kent



**Università
degli Studi
di Ferrara**



**UNIVERSITÀ
DEGLI STUDI
DI PADOVA**

- Introduction to EIC-PATHFINDER TECHNO-CLS project
 - » Gamma-ray Crystal-based Light Sources (CLS): basic ideas
 - » Overview of the main tasks of the Working Package 2 (WP2)
- WP2 Theory and modelling
 - » Task 2.1
 - » Task 2.2
 - » Tasks 2.3 and 2.4
- Conclusions and outlook

Selected examples of the novel gamma-ray Crystal based Light Sources (CLSs). Black circles and lines mark atoms of crystallographic planes, wavy curves show trajectories of the channeling particles, shadowed areas refer to radiation.

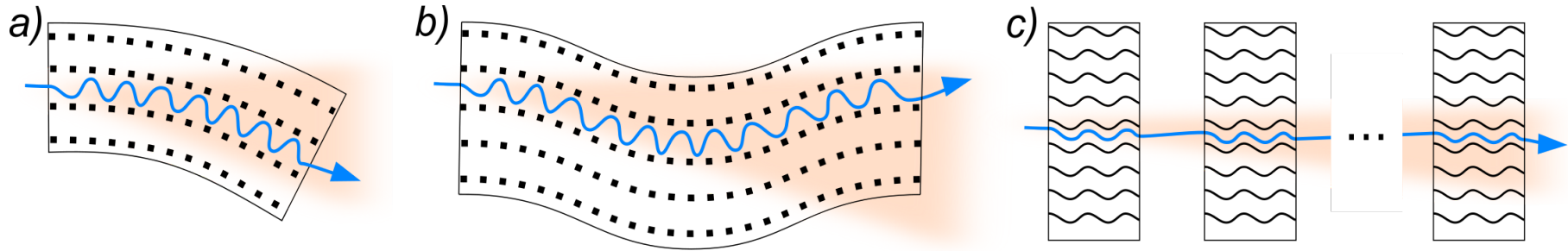
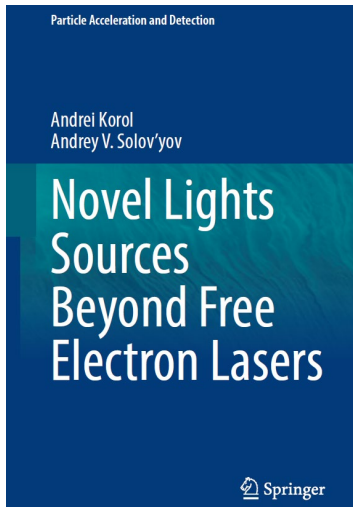
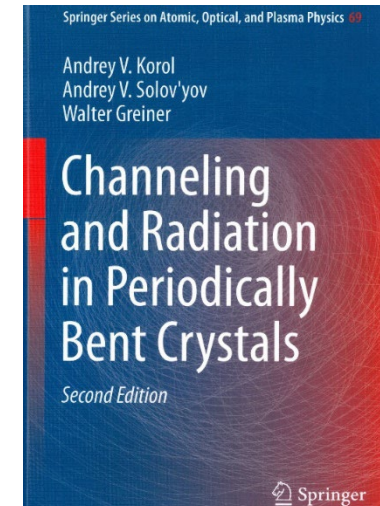


Figure from A.V. Korol, and A.V. Solov'yov, Eur. Phys. J. D (2020) 74: 201



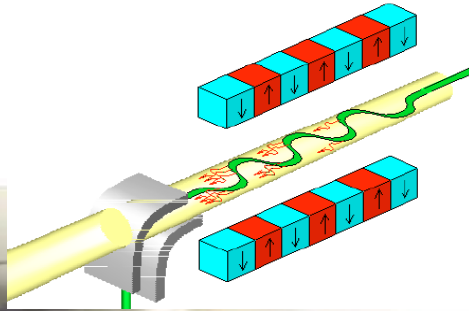
- A.V. Korol, A.V.Solov'yov, *Novel Lights Sources Beyond Free Electron Lasers*, Particle Acceleration and Detection series, Springer Nature Switzerland, Cham (2022)
- A.V. Korol and A.V. Solov'yov, *Crystal-based intensive gamma-ray light sources* (Topical Review), Eur. Phys. J. D, vol. 74, 201 (2020)
- A.V. Korol, G.B. Sushko, and A.V. Solov'yov, *All-atom relativistic molecular dynamics simulations of channeling and radiation processes in oriented crystals* (Topical Review), Eur. Phys. J. D, vol. 75, 107 (2021)
- A.V. Korol, A.V. Solov'yov, Greiner, *Channeling and Radiation in Periodically Bent Crystals*, Second Edition, Springer-Verlag, Berlin, Heidelberg (2014)



Crystalline vs magnetic undulator

Magnetic undulator:

$\lambda_u \sim 1 \text{ cm}$, $\hbar\omega \sim 10 \text{ keV}$



Crystalline undulator:

$\lambda_u \sim 10 \mu\text{m}$, $\hbar\omega \sim 0.1 \dots 10 \text{ MeV}$

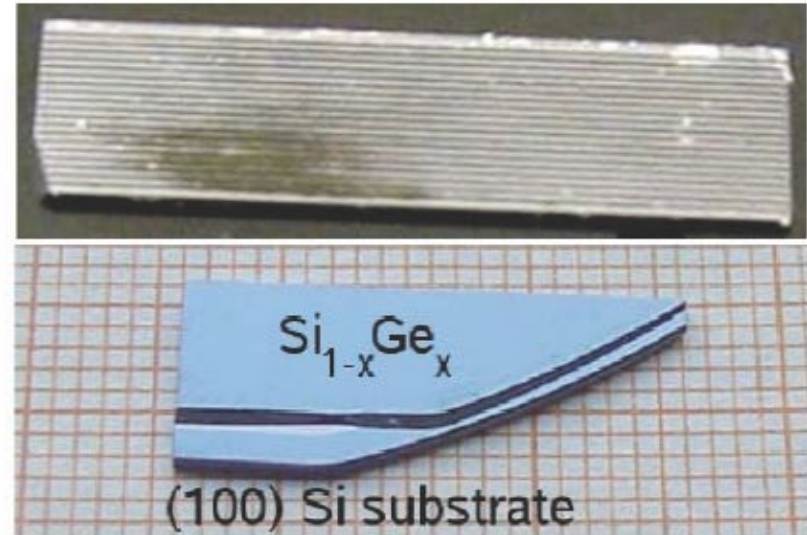


Fig. 1.3 *Left:* Magnetic undulator for the X-ray laser XFEL [179]. The picture is taken from [180]. *Right top:* laser-ablated diamond crystal. The crystal size is $4 \times 2 \times 0.3 \text{ mm}^3$. The undulator period is $\lambda_u = 50 \mu\text{m}$. The picture is taken from [74]. *Right bottom:* a $\text{Si}_{1-x}\text{Ge}_x$ superlattice crystalline undulator with four periods. Periodically varied Ge content (from $x = 0$ to $x_{\text{max}} = 0.5\%$) gives rise to the undulator period $\lambda_u = 50 \mu\text{m}$. The picture is courtesy of J.L. Hansen, A. Nylandsted and U. Uggerhøj (University of Aarhus).

Brilliance of a photon source relates the number of photons of a given energy emitted per unit time interval, unit source area, unit solid angle and per bandwidth:

$$B_n = \frac{\Delta N_{\omega_n}}{10^3 (\Delta \omega_n / \omega_n) (2\pi)^2 \varepsilon_x \varepsilon_y} \frac{I}{e}$$

n – harmonic number

$\omega_n, \Delta \omega_n$ – energy and width of the n th harmonic

$\Delta \omega_n / \omega_n$ – bandwidth (=BW)

ΔN_{ω_n} – number of photons with

$$\omega \in \left[\omega_n - \Delta \omega_n / 2, \omega_n + \Delta \omega_n / 2 \right]$$

I – electric current of the beam

$\varepsilon_{x,y}$ – emittance of the photon source along

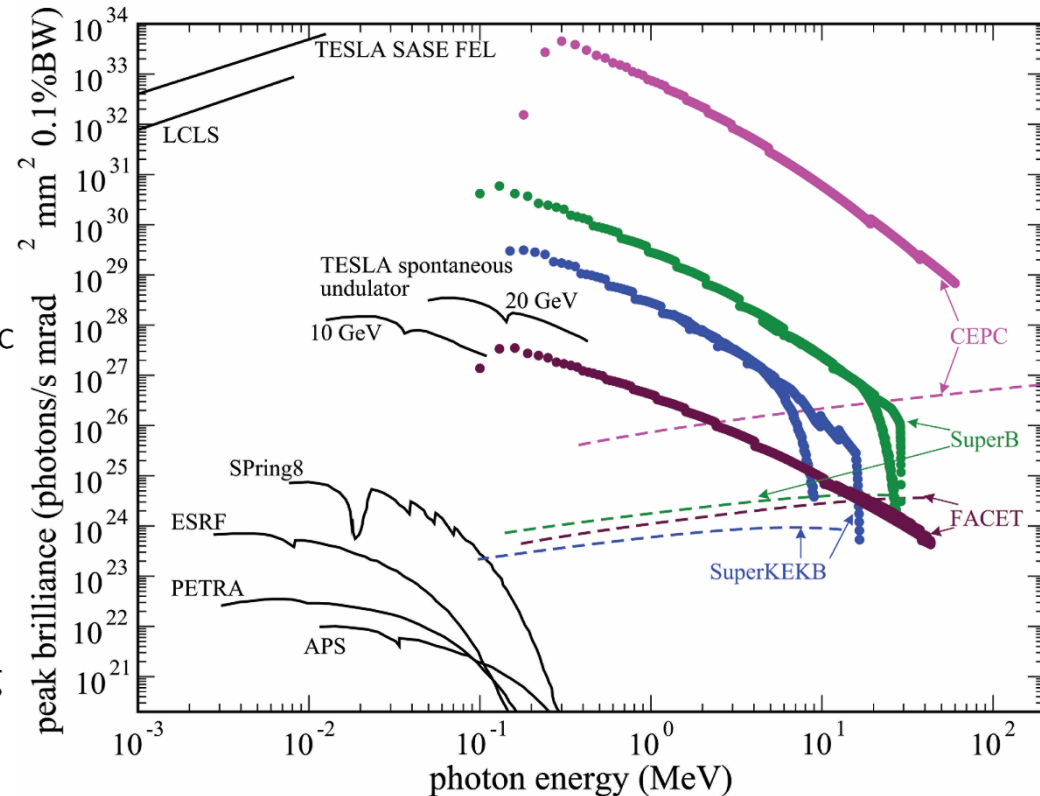
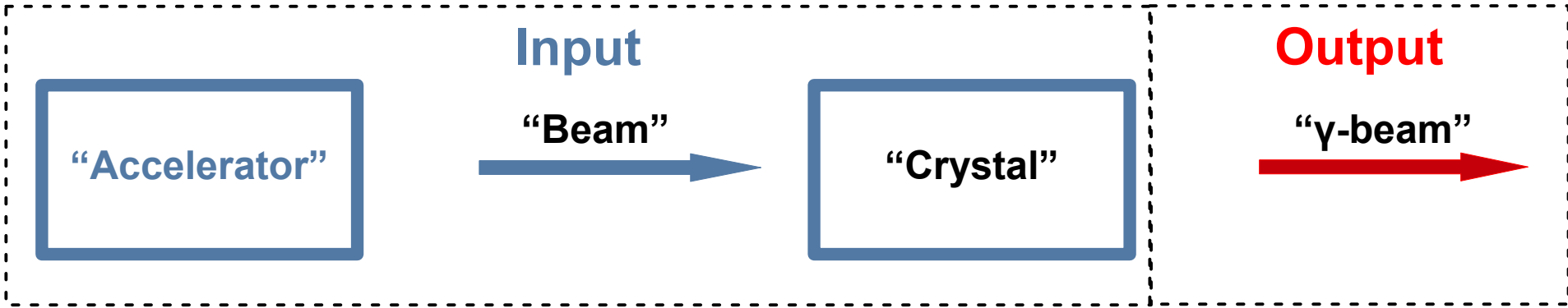


Fig. 7. Peak brilliance of superradiant CUR (thick solid curves) and spontaneous CUR (dashed lines) from diamond(110) CUs calculated for the SuperKEKB, SuperB, FACET-II and CEPC positron beams versus modern synchrotrons, undulators and XFELs. The data on the latter are taken from reference [8].

A.V Korol, A.V Solov'yov, Eur. Phys. J. D (2020) 74: 201

Prototypes of gamma-ray CLSs



Principal elements:

- Type of accelerator
- Apparatus
- Beam line

- Infrastructure

Characterisation of the beam:

- Type of projectile
- Energy and energy spread
- Size
- Emittance
- Current

Relevant issues:

- Crystal manufacture;
- Structure characterisation
- Crystal manipulation
- Channeling experiments
- Advanced simulations

Experimental and theoretical characterisation of the radiation:

- Spectral-angular distribution
- Number of photons
- Brilliance
- Power

- O2.1 Computer modelling of BC & PBC structures fabricated by means of different technologies.
- O2.2 Multiscale simulations of particle propagation in LC, BC & PBC.
- O2.3 Atomistic level characterisation of related phenomena (multiple scattering, channeling, dechanneling, rechanneling, volume reflection and capture, energy losses).
- O2.4 Characterisation of radiation emitted in CLS under conditions matching existing experimental setups and those beyond.
- O2.5 Comparison of the results of simulations with experiment.
- O2.6 Characterisation of CLSs



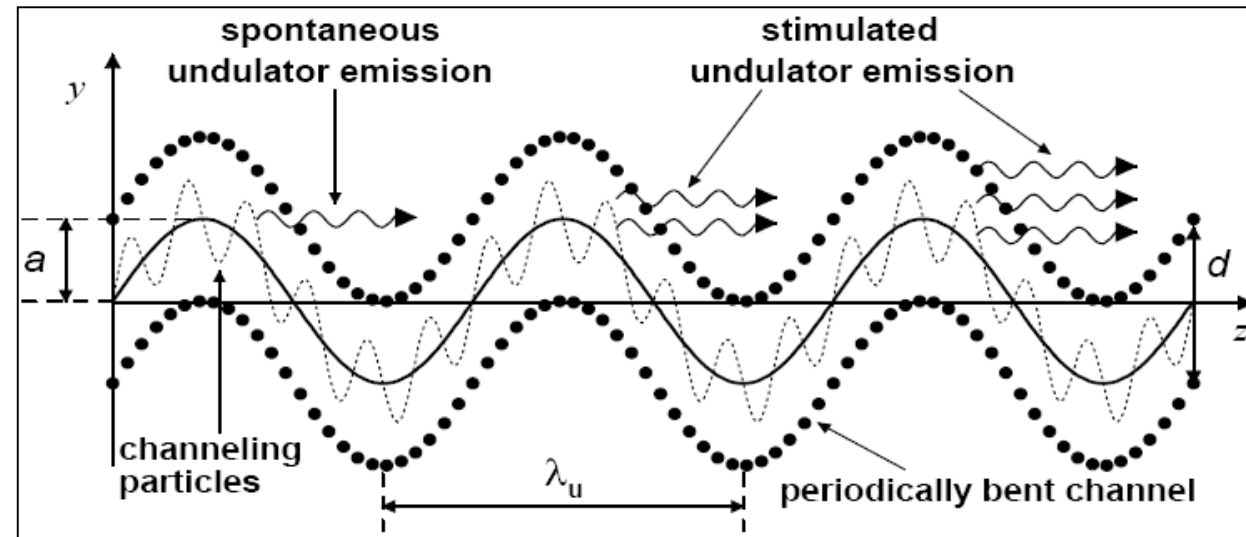
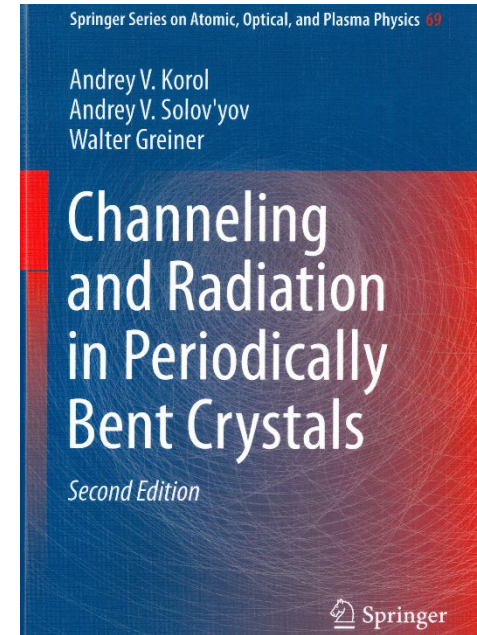
T2.1: (HMU, MBN-RC)

- **Modelling of *crystal structure modification due to AW excitation* by means of (i) a piezoelectric transducer, (ii) a laser pulse.**
- Verification of the results against the experiment.
- **Determination of the optimal parameters of the piezoelectric element/laser pulse to achieve highest photon yield.**

Radiation from a crystalline undulator

Basic idea (Korol, Solov'yov, Greiner, J.Phys.G, v.24, L45 (1998); **reviews:** *International Journal of Modern Physics E*, v.8, p.49-100 (1999); v.13, p.867-916 (2004)); PRL, 98, 164801, (2007); **Monograph**, Second Edition, Springer–Verlag, Berlin, Heidelberg (2014)

The radiation is generated by a bunch of ultra-relativistic positrons ($\epsilon=0.5...10$ GeV) channeling in a crystal along periodically bent crystallographic planes. The periodicity of trajectories results in the undulator-type radiation due to the constructive interference of the photons emitted from similar parts of the trajectory.



$d=1...2 \text{ \AA}$ - the interplanar spacing
 $a=(10...50)d$ - the amplitude of bending
 $\lambda_u=(10^4...10^5)a$ - the period of bending



$$d \ll a \ll \lambda$$

Spectral and angular distribution of spontaneous radiation in CU

$$\frac{dE_N}{d\omega d\Omega_{\mathbf{n}}} = D_N(\eta) F(\omega; \gamma, p; \theta, \varphi)$$

Here, $F(\omega; \gamma, p; \theta, \varphi)$ is a smooth function of the arguments

$$D_N(\eta) = \left(\frac{\sin N\pi\eta}{\sin \pi\eta} \right)^2$$

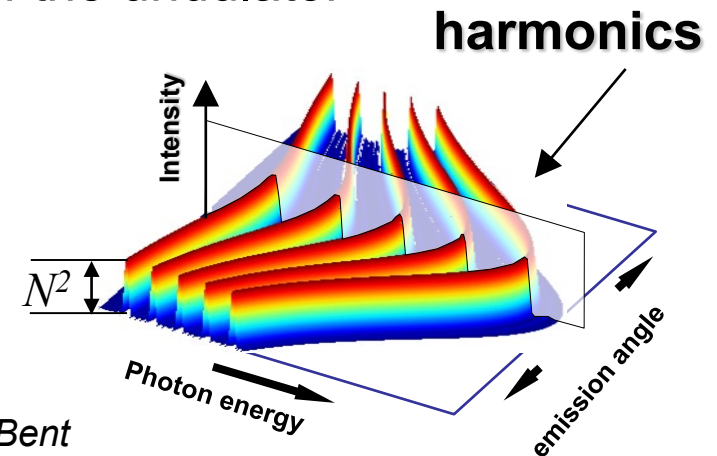
$$\omega^{(K)} = \frac{4\gamma^2 \Omega_u K}{2 + 2\theta^2 \gamma^2 + p^2}, \quad K = 1, 2, \dots$$

$$\eta = \frac{\omega}{\Omega_u} \left(\frac{1}{2\gamma^2} + \frac{\vartheta^2}{2} + \frac{p^2}{4\gamma^2} \right)$$

The characteristic frequencies (harmonics) of the undulator radiation

$$p^2 = 2\gamma^2 \frac{\dot{y}^2}{c^2}$$

p is undulator parameter
dipole regime: $p \ll 1$
non-dipole regime: $p \gg 1$



A.Korol, A.V. Solov'yov, W.Greiner, *Chan. and Rad. In Periodically Bent Crystals*, Second Edition, Springer-Verlag, Berlin, Heidelberg (2014)

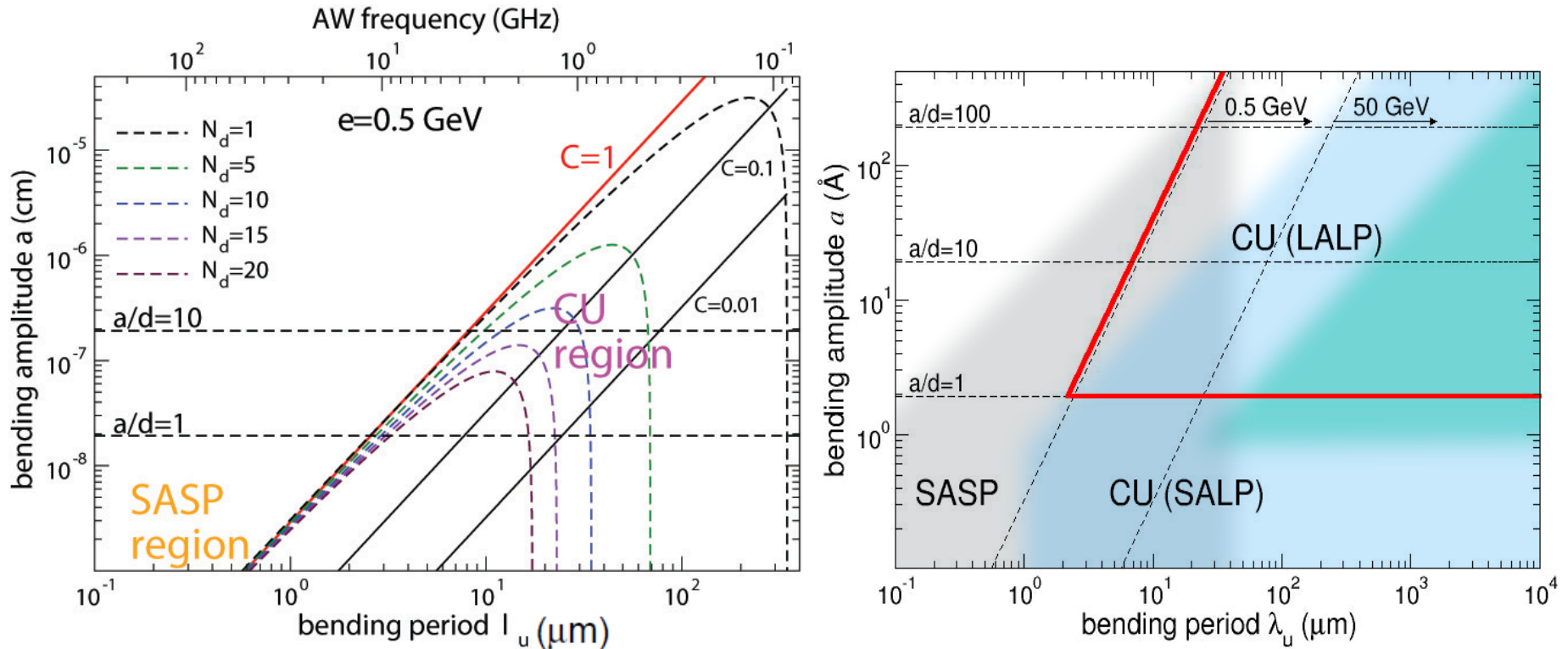
The summary of all essential conditions (Korol, Solov'yov, Greiner 1998, 2004):

$$\left\{ \begin{array}{ll} C = (2\pi)^2 \frac{\varepsilon}{qU'_{\max}} \frac{a}{\lambda^2} \ll 1 & \text{stable channeling} \\ d \ll a \ll \lambda & \text{large-amplitude regime} \\ N = \frac{L}{\lambda} \gg 1 & \text{large number of undulator periods} \\ L \leq \min [L_d(C), L_a(\omega)] & \text{account for the dechanneling} \\ & \text{and photon attenuation} \\ \frac{\Delta\varepsilon}{\varepsilon} \ll 1 & \text{low radiative losses} \end{array} \right.$$

If these are met then:

- within the length L the particle experiences stable planar channeling
- characteristic energies of the undulator and channeling radiation are well separated
- intensity of the undulator radiation is higher than that of the channeling radiation.
- emission spectrum is stable towards the radiative losses.

CU parameter ranges

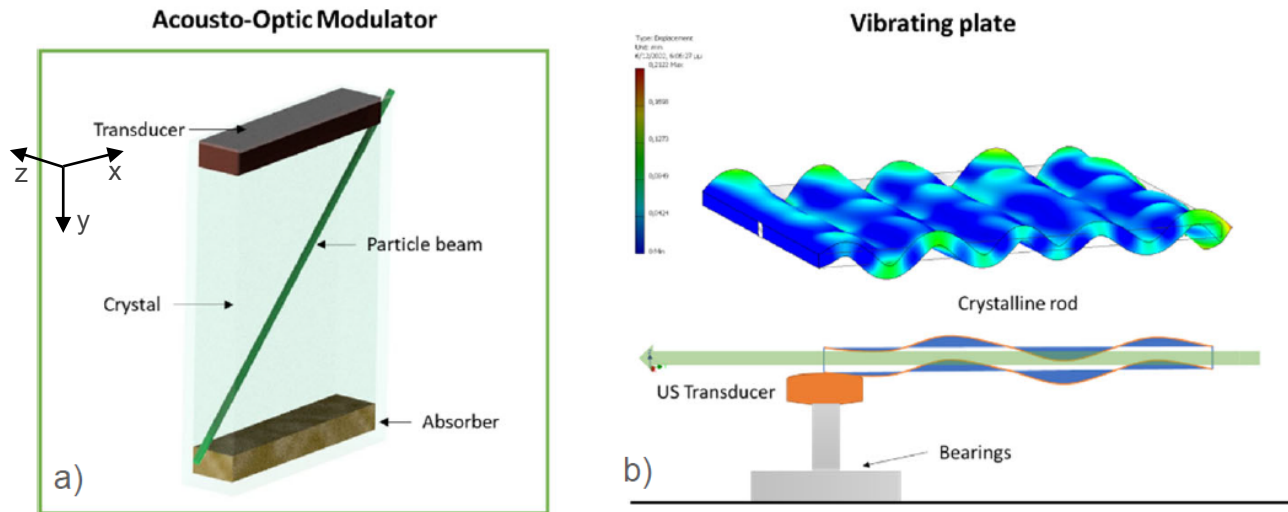


Left figure. Bending amplitude, a , vs bending period, λ , consistent with the condition $C < 1$ and calculated for various numbers of undulator periods N_d as indicated for $e=0.5$ GeV ($\gamma = 10^3$) positron channeling in Si along (110) crystallographic plane. Bending profile $y = a \sin(2\pi z/\lambda)$.

A.Korol, W.Krause, A.Solov'yov, W.Greiner, J.Phys.G: Nucl.Part.Phys., v.26, L87-L95 (2000);

From A.Korol, A.Solov'yov, W.Greiner, Chan. and Rad. In Periodically Bent Crystals, Second Edition, Springer-Verlag, Berlin, Heidelberg (2014);

Right figure. Shadowing indicates the ranges accessible by means of modern technologies: superlattices (grey), surface deformations (green), AWs (blue); **From A.V. Korol and A.V. Solov'yov, Eur. Phys. J. D, vol. 74, 201 (2020)**



A 20 GeV positron beam (red arrow) of the size $\sigma=150 \mu\text{m}$ (SLAC specification) enters the crystal. For these geometries, the **two FEM simulation sets** have been performed (HMU).

Figure 2.1.1: Schematic diagrams of novel acoustically excited crystalline undulator layouts, a) Acousto-Optic Modulator–type (AOM) AW CU and b) Vibrating Plate–type (VP) AW CU.

SET1: Harmonic pressure P ($P_{\text{max}}=4 \text{ MPa}$; $\nu=10$ and 40 MHz) is applied on the upper XZ plane. Boundary conditions: (i) free boundaries on the YZ and XY planes; (ii) non-reflective (absorber) boundaries on the lower XZ plane.

SET2: Harmonic pressure ($P_{\text{max}}=4 \text{ MPa}$; $\nu=10 \text{ MHz}$) is applied on the upper XZ plane. Boundary conditions: (i) simply supported plate boundaries on the YZ and XY planes; (ii) non-reflective (absorber) boundary conditions at the bottom XZ plane.

Work in progress: MBN-RC & HMU.

SET 1: Excitation frequency 40 MHz

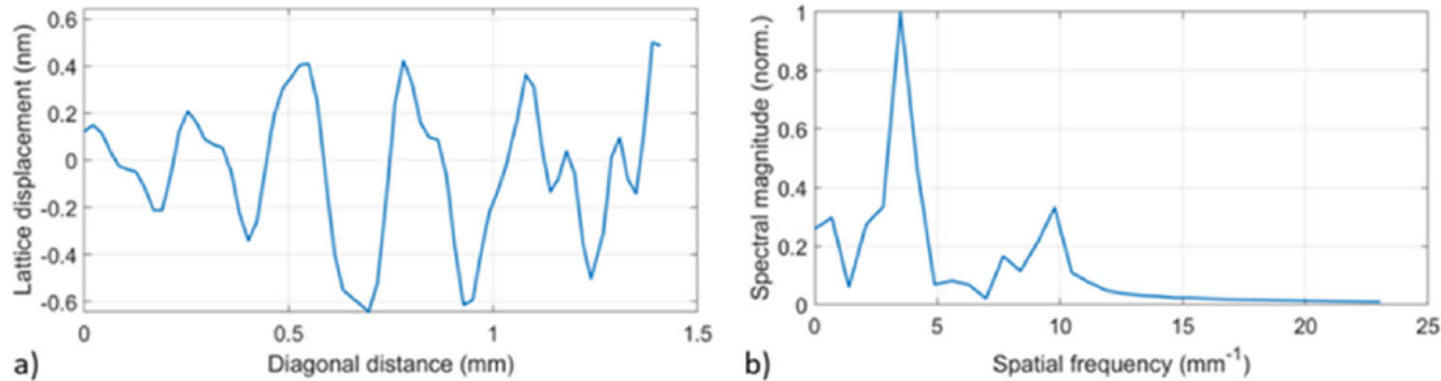
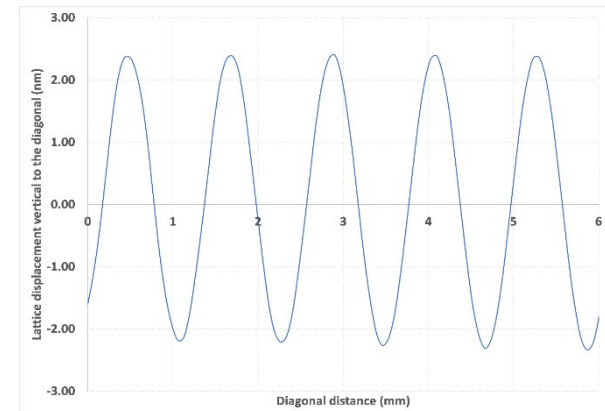


Figure 2.1.3: FEM simulations of the acoustically induced lattice modulation of the Si1 crystal excited with 42 MHz, 4 MPa harmonic pressure a) space domain, b) spatial frequency domain.

SET 2: Excitation frequency 10 MHz

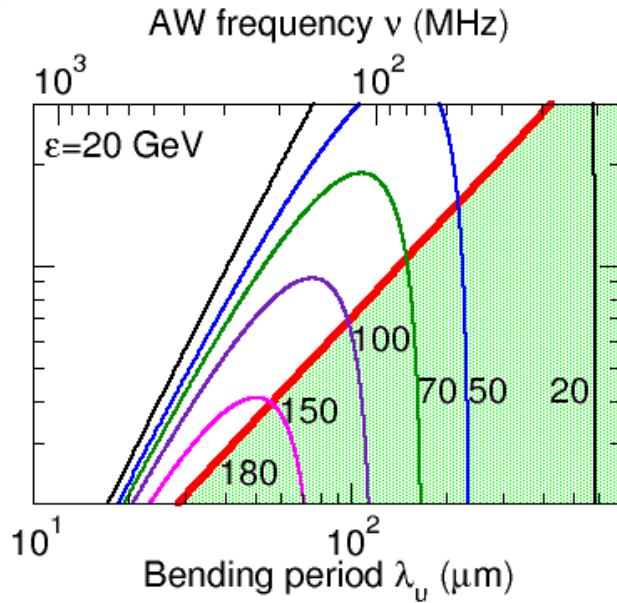
Bending profiles along the central path

Potential experimental realization of SET 2 can be difficult and require further feasibility investigation.

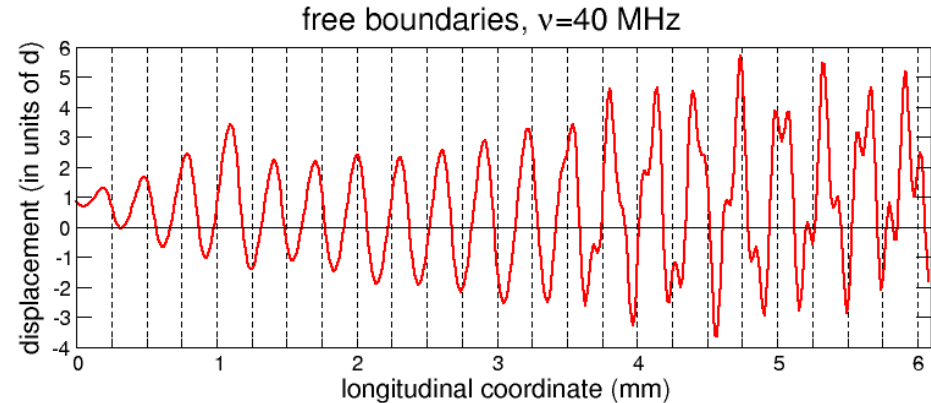
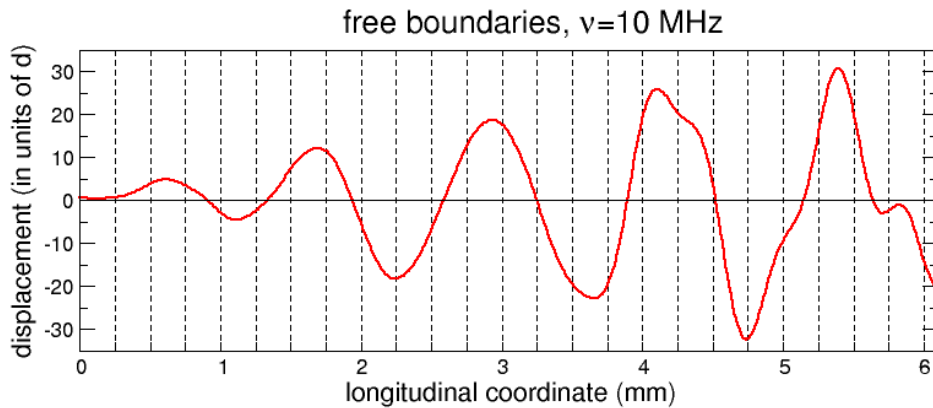


CU via AW excitation for 20 GeV e⁺

Work in progress: MBN-RC & HMU.



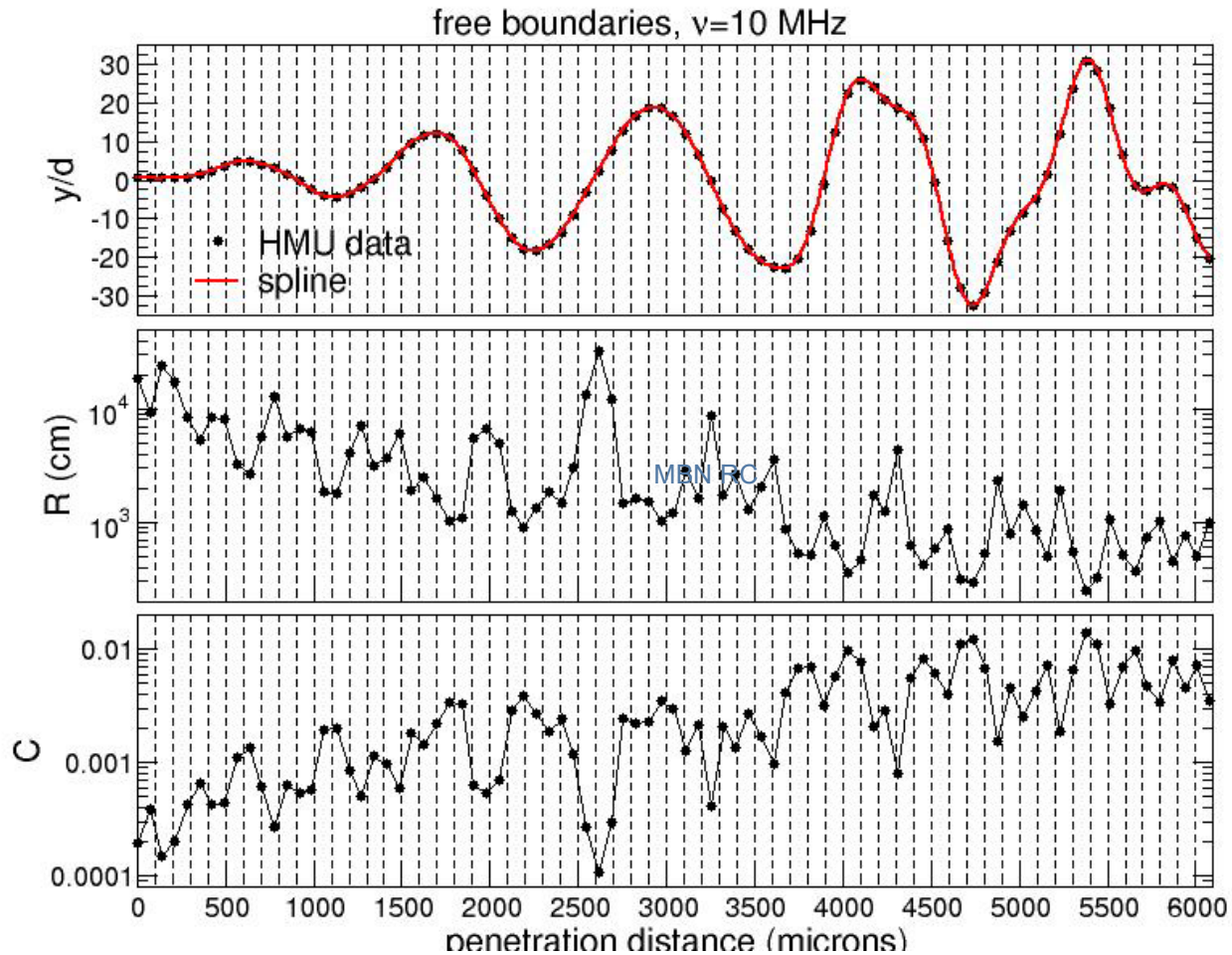
Left figure: Ranges of bending period λ_u and amplitude $a > d = 1.92$ Å to be probed to construct a Si(110)-based CU for $\epsilon = 20$ GeV positrons. The CU can be considered in the shadowed domain lying below the red line. Integers indicate the number of undulator periods within the dechanneling length. The upper horizontal axis in shows the frequency of the AW transmitted along the $\langle 100 \rangle$ axial direction, that causes periodic bending of the (110) planes.



Bending profiles of (110) planes in Si due to AW with free boundary conditions. Left panel corresponds to the AW frequency 10 MHz, right panel – to 40 MHz.



SET 1: Excitation frequency 10 MHz

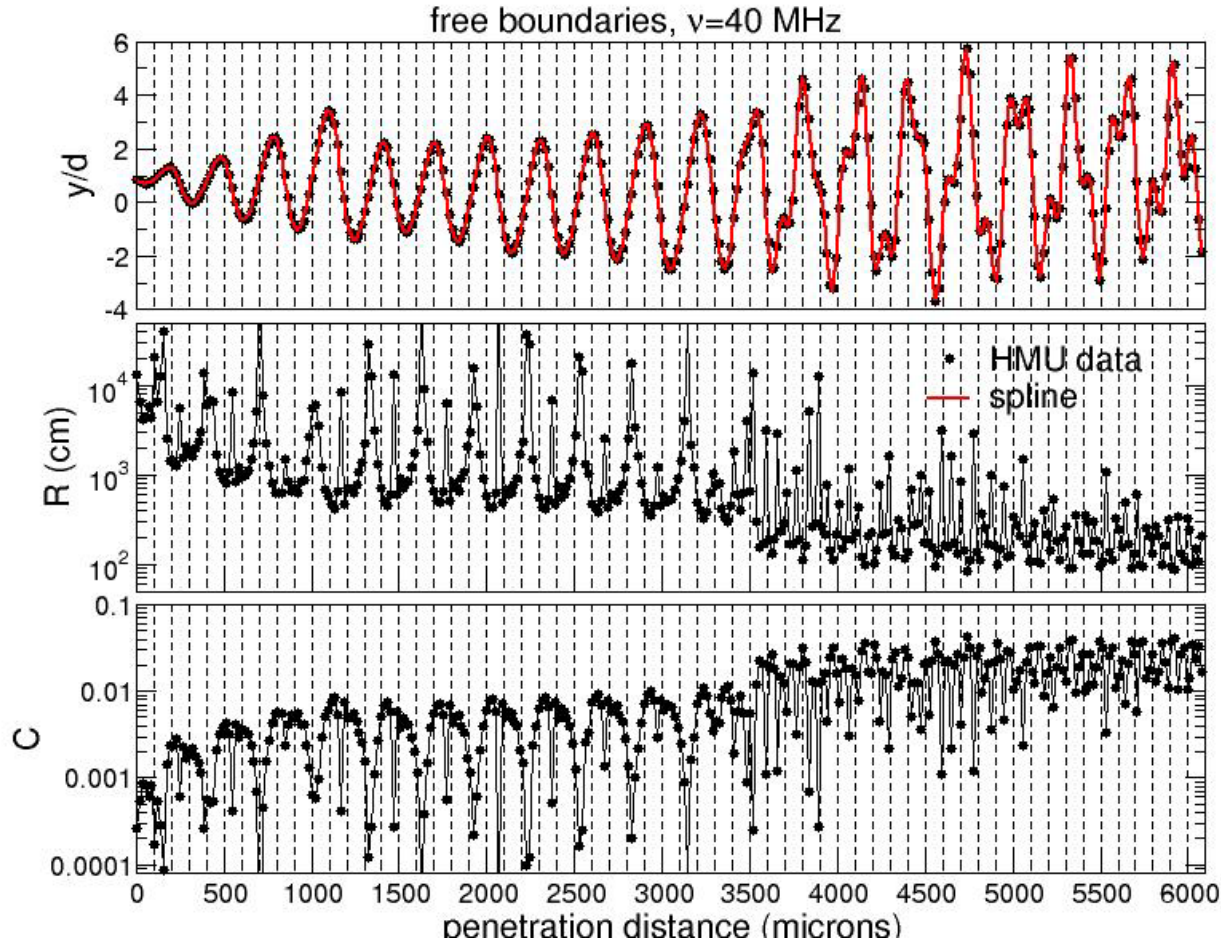


Work in progress:
MBN-RC & HMU.

Top: Bending profiles of (110) planes in Si due to AW. Middle: Local curvature radius.
Bottom: Bending parameter C =centrifugal force / interplanar force.



SET 1: Excitation frequency 40 MHz



Work in progress:
MBN-RC & HMU.

Top: Bending profiles of (110) planes in Si due to AW. Middle: Local curvature radius. Bottom: Bending parameter C =centrifugal force / interplanar force.



T2.2 (UoK, MBN-RC, UNIFE, UNIPD, ESRF)

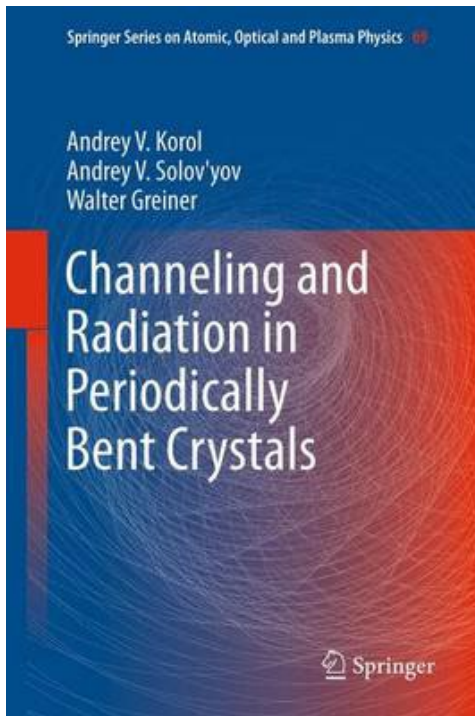
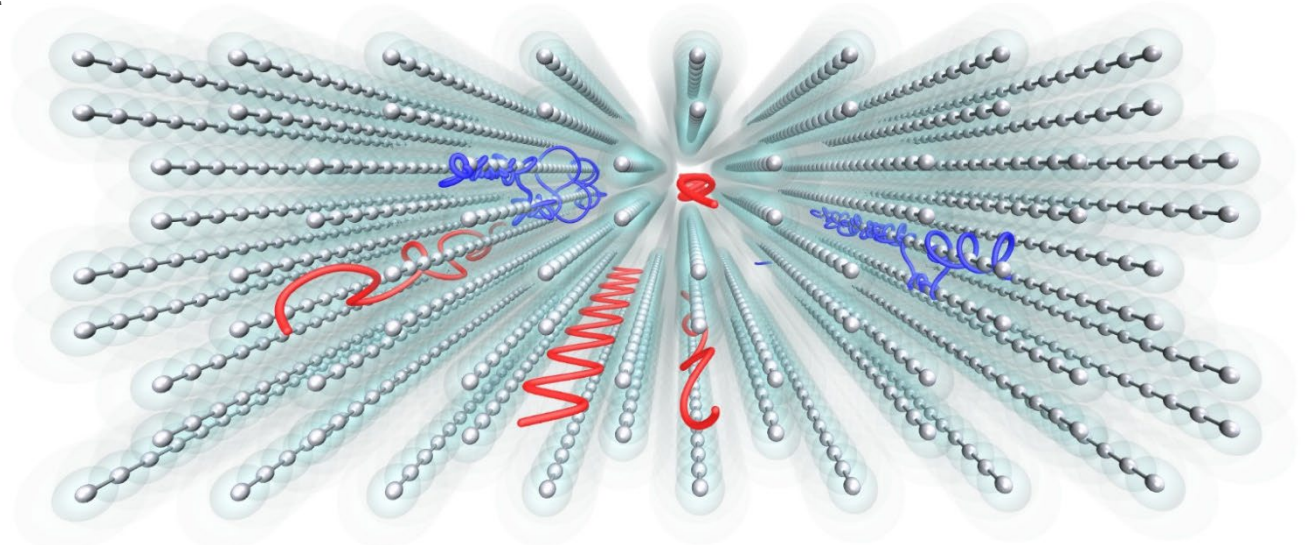
- ***Atomistic modelling* of Si- & diamond-based BC and PBC fabricated via different technologies.**
- **Studying the processes responsible for crystal imperfections.**
- Comparison with the data on experimental characterization.

Simulation of motion of relativistic particles in MBN Explorer is based on relativistic equations of motion.

$$\begin{cases} \dot{\mathbf{v}} = \frac{1}{m\gamma} \left(\mathbf{F} - \mathbf{v} \frac{(\mathbf{F} \cdot \mathbf{v})}{c^2} \right) \\ \dot{\mathbf{r}} = \mathbf{v} \end{cases}$$

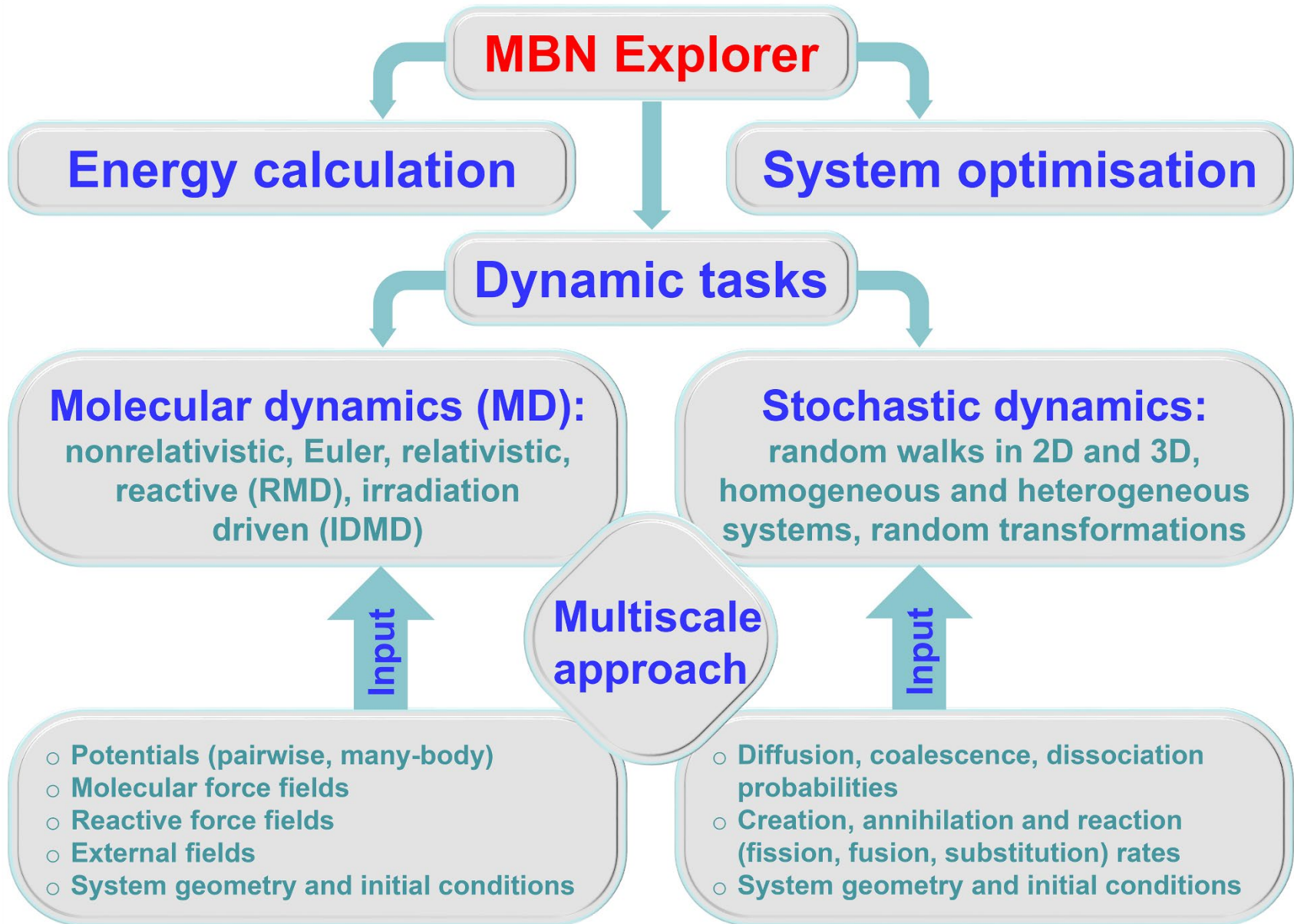
This system of equations is strongly nonlinear and requires the use of high-order integrator in order to be solved correctly

$$\gamma = \frac{1}{\sqrt{1 - v^2/c^2}}$$



The developed approach (G.B. Sushko, V.G. Bezchastnov, I.A. Solov'yov, A.V. Korol, W. Greiner, A.V. Solov'yov, *Journal of Computational Physics*, 252, 404 (2013)) is not restricted to the crystalline medium and is applicable to describe the propagation of ultra-relativistic projectile in an arbitrary medium.

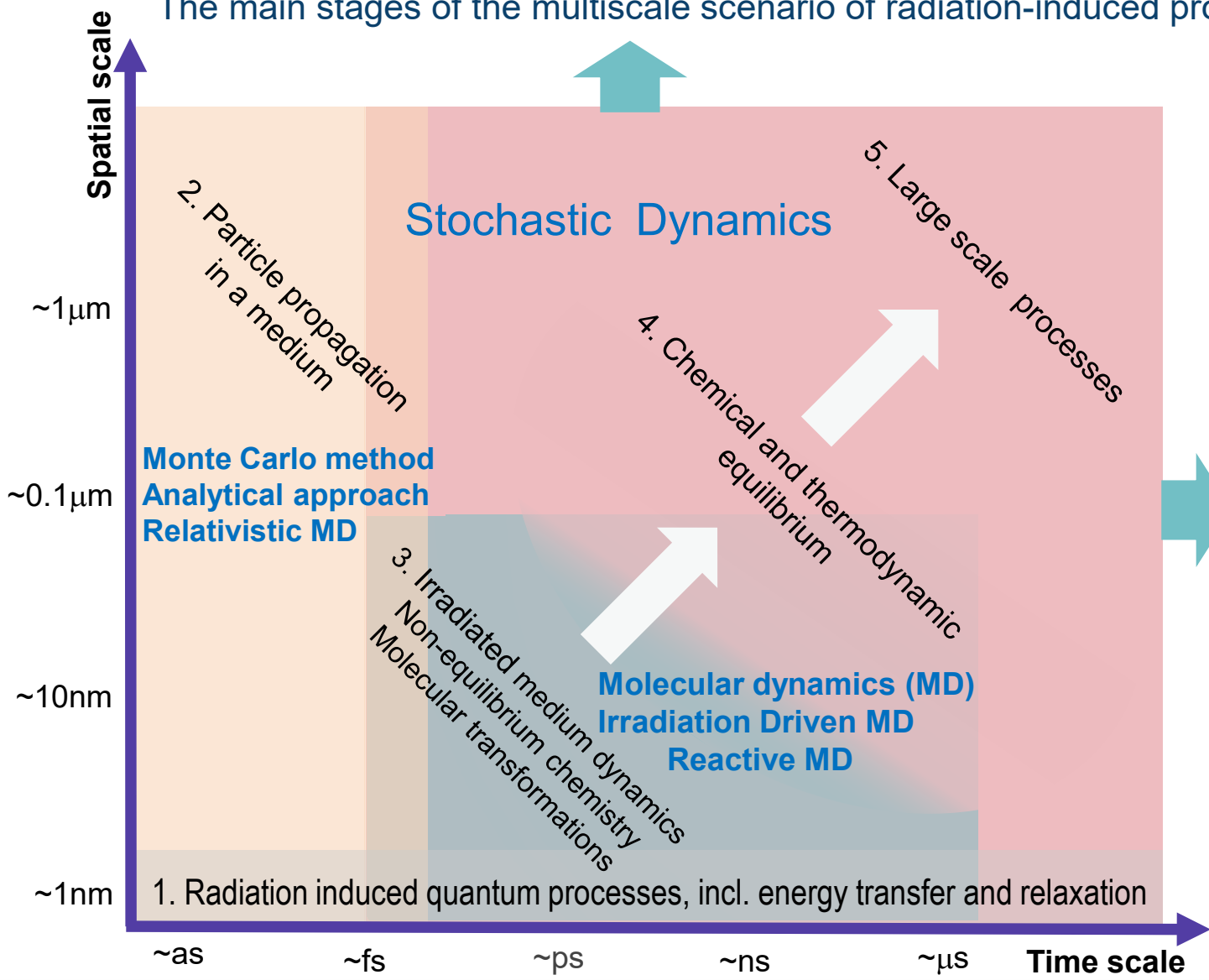
A.V. Korol, G.B. Sushko, and A.V. Solov'yov, All-atom relativistic molecular dynamics simulations of channeling and radiation processes in oriented crystals (Topical Review), *Eur. Phys. J. D*, vol. 75, 107 (2021)



Multiscale theory of irradiated MesoBioNano (MBN) systems



The main stages of the multiscale scenario of radiation-induced processes



A.V. Solov'yov, A.V. Verkhovtsev, N Mason, I.A. Solov'yov, et al, *Condensed matter systems exposed to radiation: the multiscale theory, simulations and experiment, Roadmap paper*, [arXiv:2311.13402](https://arxiv.org/abs/2311.13402) [[physics.chem-ph](https://arxiv.org/archive/physics)], *Chemical Reviews* (2024, online ahead of print, <https://pubs.acs.org/doi/10.1021/acs.chemrev.3c00902>) (impact factor 62);

A.V. Solov'yov (ed.), *Advances in Atomic and Molecular Physics at the interfaces with Natural Sciences, Technology and Medicine*, World Scientific, in preparation, 2024



CHEMICAL REVIEWS

pubs.acs.org/CR

(2024), online ahead of print,
<https://pubs.acs.org/doi/10.1021/acs.chemrev.3c00902>

Review

1 Condensed Matter Systems Exposed to Radiation: Multiscale Theory, Simulations, and Experiment

3 Andrey V. Solov'yov,* Alexey V. Verkhovtsev, Nigel J. Mason, Richard A. Amos, Ilko Bald,
4 Gérard Baldacchino, Brendan Dromey, Martin Falk, Juraj Fedor, Luca Gerhards, Michael Hausmann,
5 Georg Hildenbrand, Miloš Hrabovský, Stanislav Kadlec, Jaroslav Kočíšek, Franck Lépine, Siyi Ming,
6 Andrew Nisbet, Kate Ricketts, Leo Sala, Thomas Schlathöler, Andrew Wheatley, and Ilia A. Solov'yov*

Cite This: <https://doi.org/10.1021/acs.chemrev.3c00902>

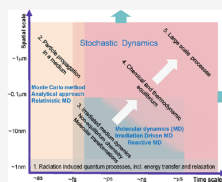
Read Online

ACCESS |

Metrics & More

Article Recommendations

ABSTRACT: This roadmap reviews the new, highly interdisciplinary research field studying the behavior of condensed matter systems exposed to radiation. The Review highlights several recent advances in the field and provides a roadmap for the development of the field over the next decade. Condensed matter systems exposed to radiation can be inorganic, organic, or biological, finite or infinite, composed of different molecular species or materials, exist in different phases, and operate under different thermodynamic conditions. Many of the key phenomena related to the behavior of irradiated systems are very similar and can be understood based on the same fundamental theoretical principles and computational approaches. The multiscale nature of such phenomena requires the quantitative description of the radiation-induced effects occurring at different spatial and temporal scales, ranging from the atomic to the macroscopic, and the interlinks between such descriptions. The multiscale nature of the effects and the similarity of their manifestation in systems of different origins necessarily bring together different disciplines, such as physics, chemistry, biology, materials science, nanoscience, and biomedical research, demonstrating the numerous interlinks and commonalities between them. This research field is highly relevant to many novel and emerging technologies and medical applications.



22 CONTENTS

24	1. Introduction		
25	1.1. Condensed Matter Systems Exposed to Radiation	B	
26	1.2. Radiation Modalities	B	
27	1.3. Radiation Conditions	C	
28	1.4. Common Features in the Response of Condensed Matter Systems to Radiation	C	
29	1.5. Multiscale Scenario of Radiation-Induced Processes	C	
30	1.6. Multiscale Scenarios for Clustering, Self-Assembly, Structure Formation, and Growth Processes in Condensed Matter Systems	D	
31	1.7. Multiscale Scenario for Radiation-Driven Processes	E	
32	1.8. Multiscale Scenario for Radiation Damage to Biological Systems	F	
33	1.9. Important Applications in Technology and Medicine	H	
34	2. Multiscale Theory of Condensed Matter Systems Exposed to Radiation: The Main Concept	I	
35	2.1. Main Stages of Multiscale Scenarios for Irradiated Condensed Matter Systems	I	
36	2.2. Radiation-Induced Quantum Processes	J	
37	2.3. Particle Propagation Through a Medium	J	47
38	2.4. Irradiated Medium Dynamics and Related Phenomena	K	48
39	2.5. Post-Irradiation Chemical and Thermodynamic Equilibration	L	50
40	2.6. Large-Scale Post-Irradiation Processes	M	52
41	3. Existing Theoretical and Computational Methods and Their Limits	M	53
42	3.1. Quantum Processes	N	55
43	3.1.1. Many-Body Theory	N	56
44	3.1.2. Density Functional Theory	O	57
45	3.1.3. Time-Dependent Density Functional Theory	P	58
46	3.1.4. <i>Ab Initio</i> and Model Approaches for Calculating Scattering Cross Sections	P	60
	3.2. Particle Transport	R	61
		R	62

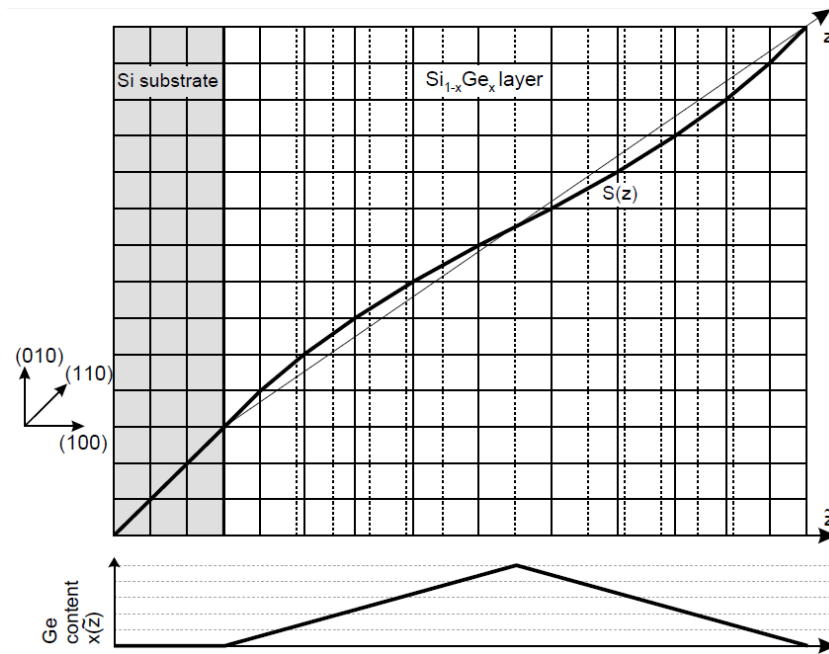
Received: December 6, 2023
Revised: May 2, 2024
Accepted: May 10, 2024

Channeling in binary crystalline structures

Bending can be achieved by variation of the dopant content in binary crystals [1].

Scheme of $\text{Si}_{1-x}\text{Ge}_x$ crystal bending due to variation of Ge content [3].

Ge and Si have different lattice parameters which leads to a deformation in $\text{Si}_{1-x}\text{Ge}_x$ [3]

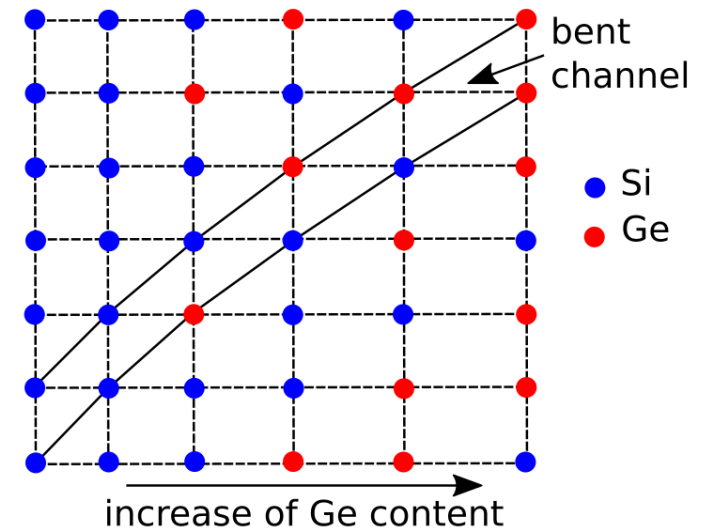


By means of MBN Explorer one can model $\text{Si}_{1-x}\text{Ge}_x$, diamond-boron etc binary systems using the MD methods.

[1] Mikkelsen & Uggerhøj, *NIMB* **160** (2000) 435

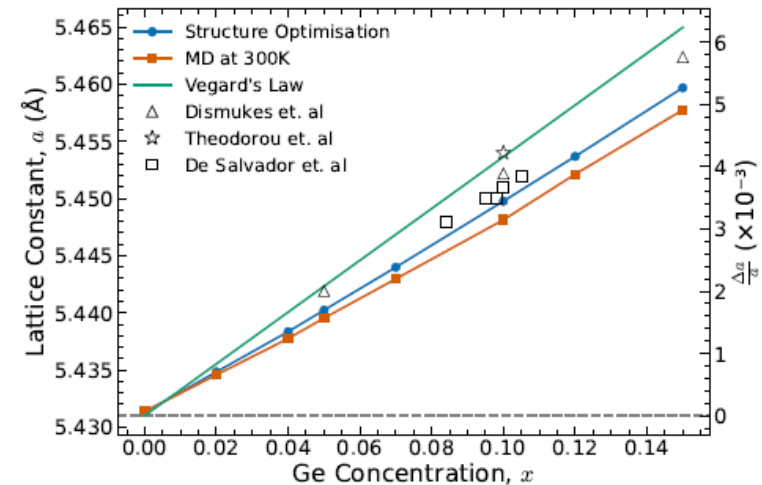
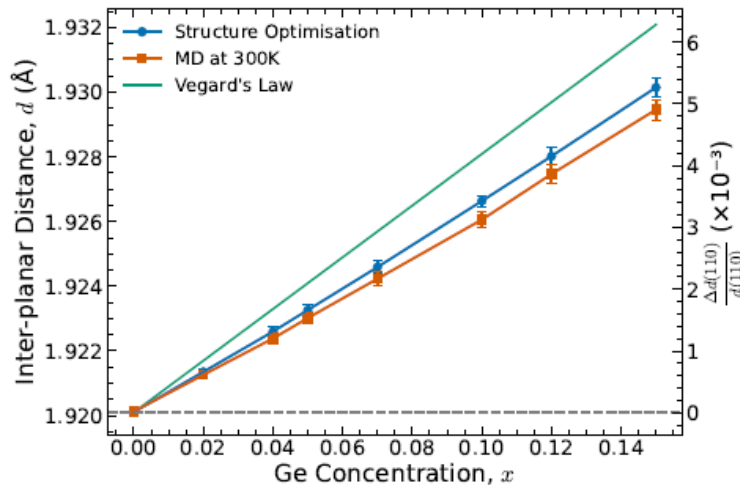
[2] Krause, Korol, Solov'yov, & Greiner, *NIMB*, **483** (2002) 455

[3] Korol, Solov'yov, Greiner, "Channeling and radiation in periodically bent crystals", Springer (2014)



Effect of doping on crystalline structure

- We have conducted a systematic analysis of the inter-planar distance change as a result of the introduction of dopant Ge atoms to a Si crystal at concentrations of $0 < x < 0.15$ ($\text{Si}_{1-x}\text{Ge}_x$) using MD simulations.
- A linear increase in inter-planar distance with Ge concentration has been observed.
- Our results are in agreement with those of experiments



Plots of the average inter-planar distance (left) and lattice constant (right) as functions of the dopant concentration. In each plot a second y axis shows the relative change in lattice constant $\Delta a/a$ or inter-planar distance $\Delta d/d$. The lattice constant is compared to experimental data (symbols) as well as the empirical Vegard's Law (the green line). The grey dashed lines show the nominal values in single Si crystals.

M. D. Dickers, G. B. Sushko, A. V. Korol, N. J. Mason, F. Fantuzzi, A. V. Solov'yov. *Dopant concentration effects on $\text{Si}_{1-x}\text{Ge}_x$ crystals for emerging light-source technologies: A molecular dynamics study*. arXiv:2402.10120v1; EPJD (in print, doi: 10.1140/epjd/s10053-024-00870-2)

Experimental and computational characterisation of PBCs

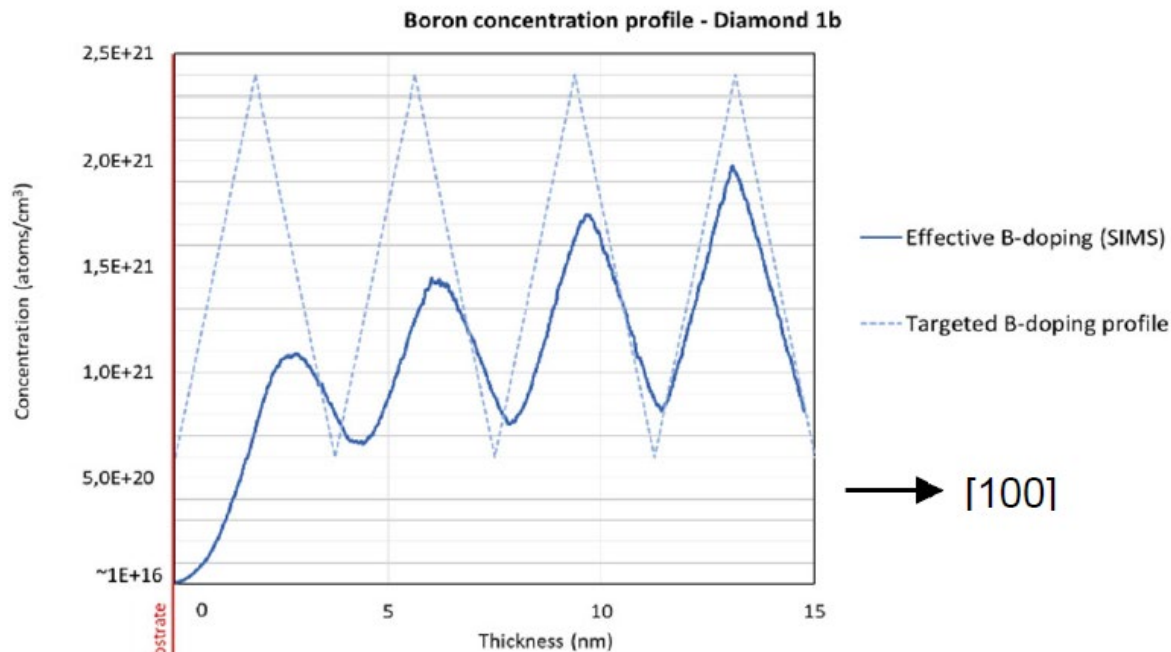


Figure 2.2.1: Boron-doping profile for diamond sample 1b.

Ref.: ESRF, 2nd year TECHNO-CLS Report.

Work in progress:
ESRF & Uni-Mainz.

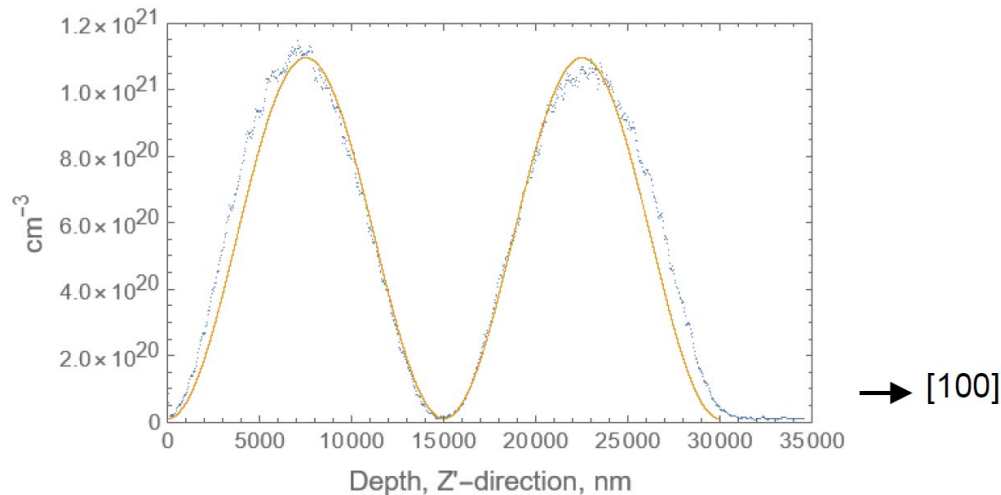


Figure 2.2.4: Comparison of the experimentally measured boron-doping for diamond sample 2a³

Ref.: ESRF and MBN RC, 2nd year TECHNO-CLS Report.

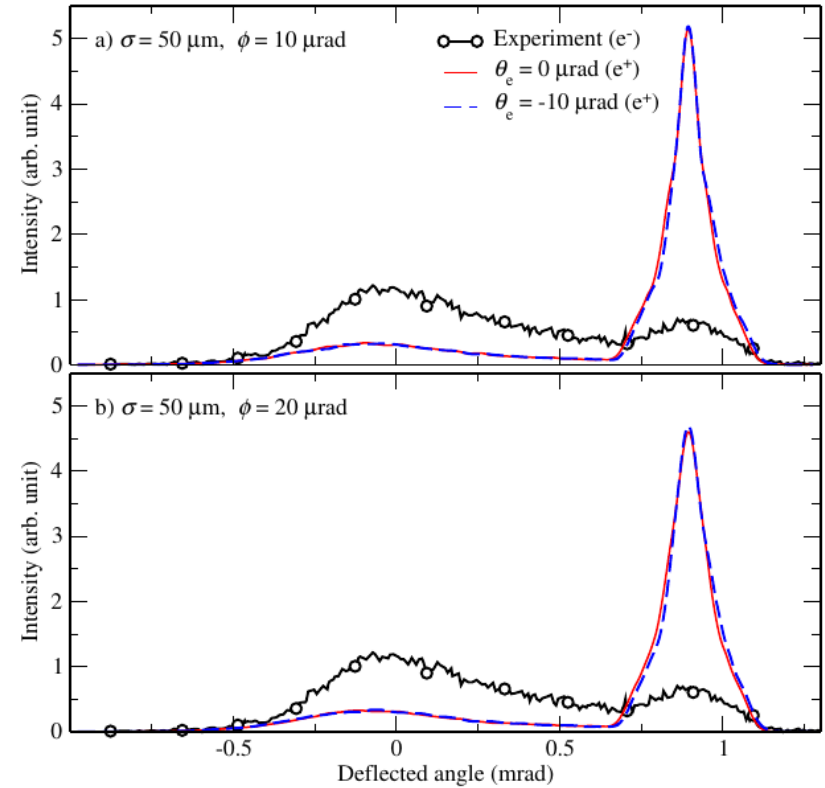
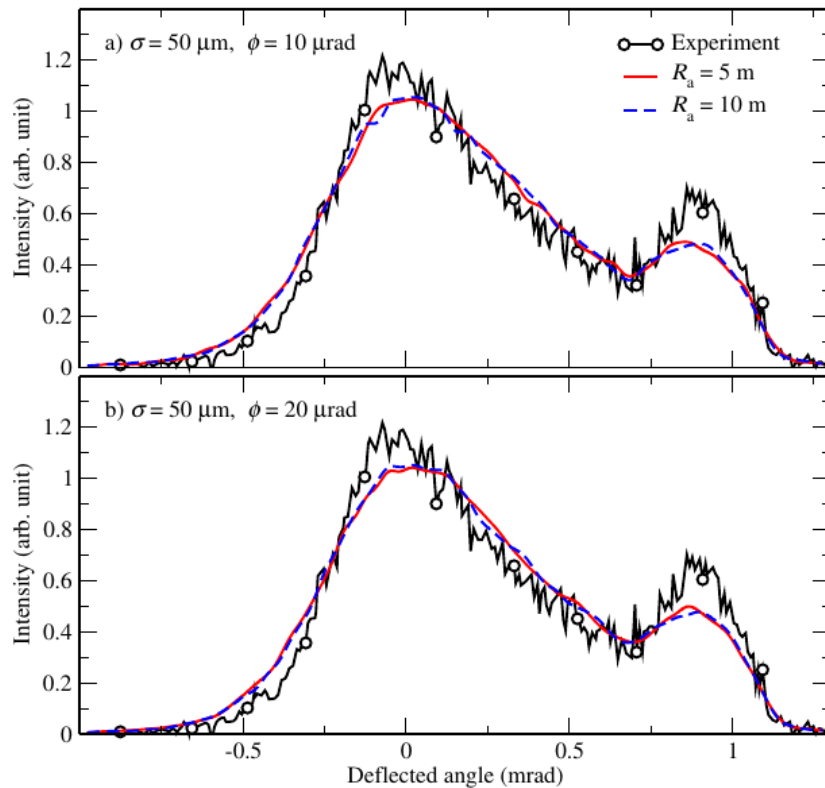
Work in progress:
ESRF & MBN-RC.



T2.3 (MBN-RC, INFN, UNIFE, Uni-Mainz)

- **Multiscale simulations of *particles propagation in LCs, BCs & PBCs* for various experimental conditions.**
- Atomistic level assessment of *related phenomena* (multiple scattering, volume reflection & capture, energy loss).
- Verification of the results with available experimental data and theoretical benchmarking for future experiments.

Simulation of e^- / e^+ deflection by bent Si crystal (@ MAMI energies)

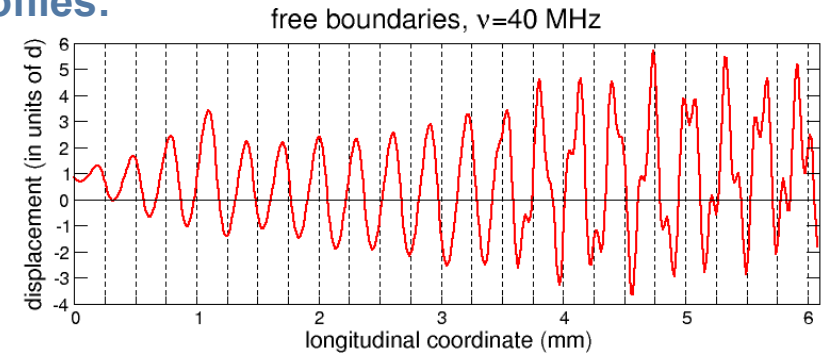
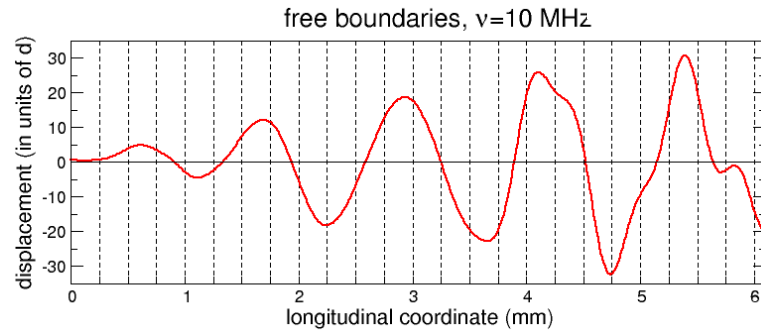


Left: Angular distribution of deflected 855 MeV *electrons* simulated for different values of the beam divergence ($\phi = 10$ and $20 \mu\text{rad}$ in the top and bottom graphs, correspondingly) and for two values of the anticlastic curvature radii R_a as indicated in the common legend shown in the top graph. All dependencies shown correspond to the beam transverse size $\sigma = 50 \mu\text{m}$. Solid line with open circles corresponds to the experimental data from Mazzolari et al, *Phys. Rev. Lett.* 112 (2014) 135503.

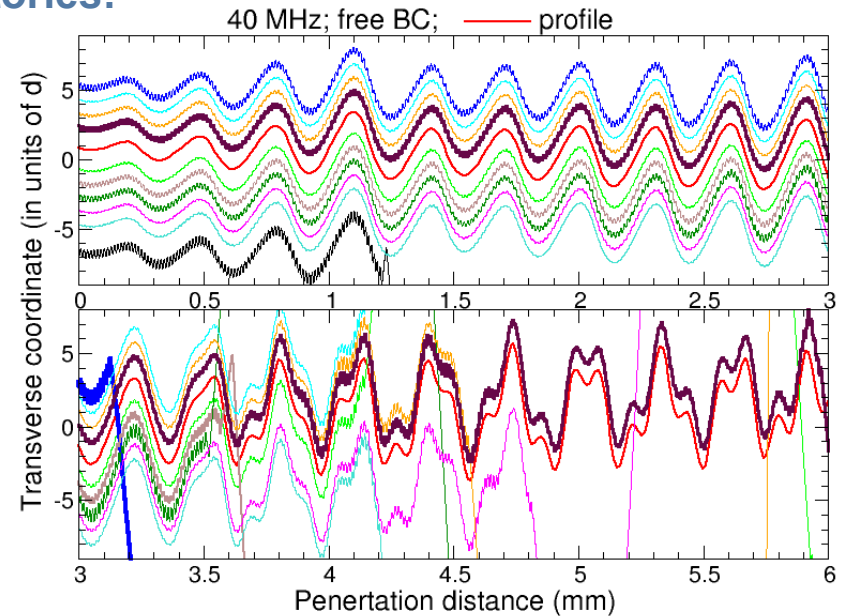
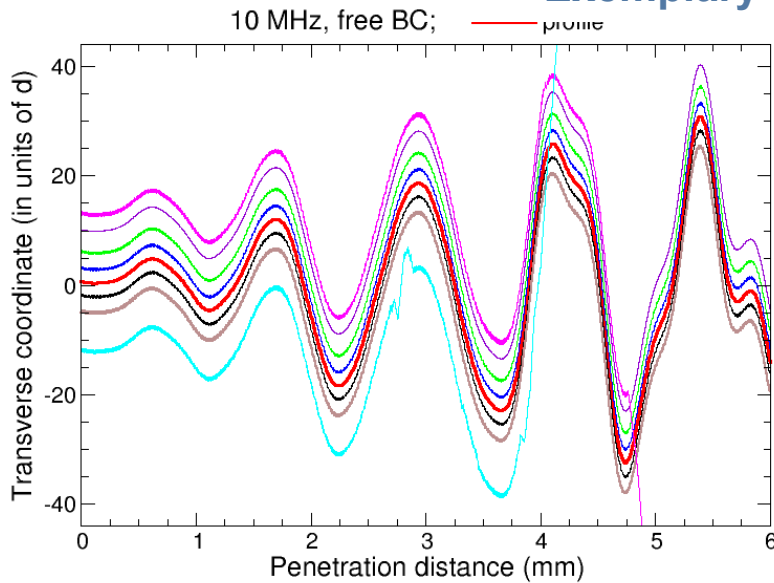
Right: Same as on the left panel but for a 855 MeV *positron* beam incident on the quasi-mosaic Si(111) crystal. All simulated distributions refer to the anticlastic curvature radius $R_a = 5 \text{ m}$. For the sake of comparison. The experimental data for electrons are also shown.

Multiscale simulations of 20 GeV e^+ in 2-6 mm thick Si crystals bent by AW

Bending profiles:



Exemplary trajectories:

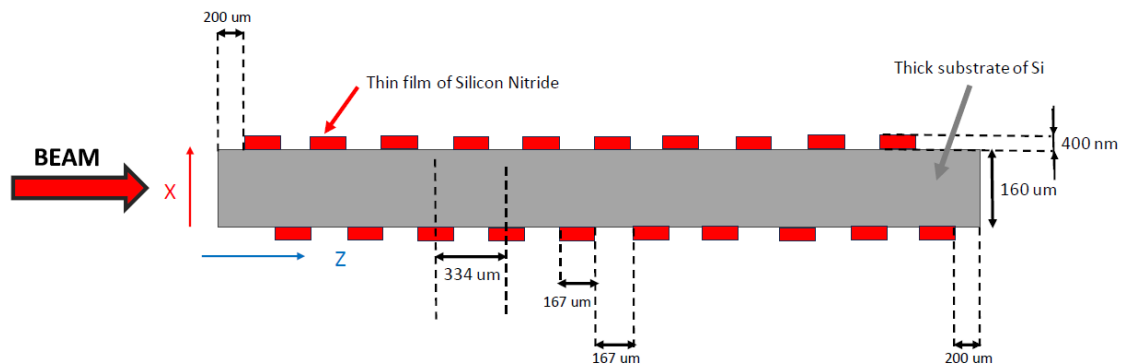


In the right figure the trajectories are shown in two segments: 0-3 mm(top) and 3-6 (bottom)

MBN-RC & HMU teams: work in progress.

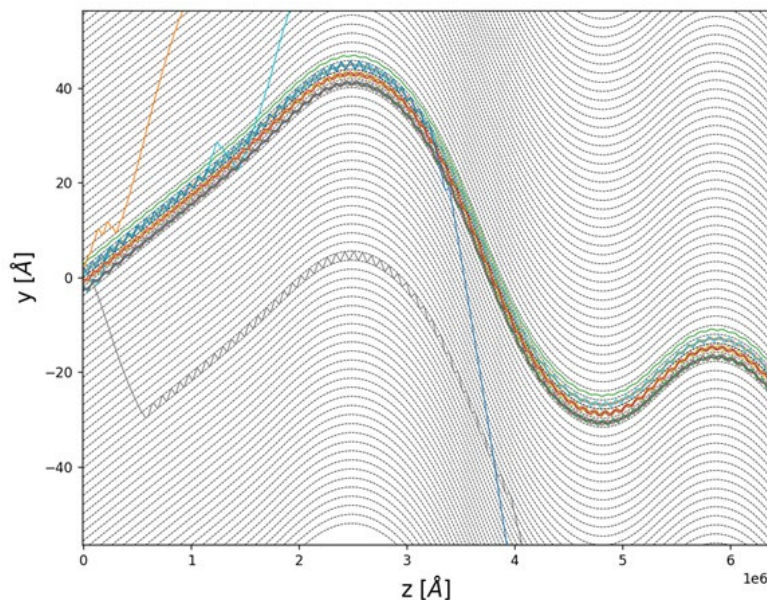
Simulations of 5-20 GeV e^+ in Si PBC

PBC Si crystal manufactures by means of surface patterning technology (UNIFE & INFN):



Exemplary trajectories:

MBN-RC, INFN & UNIFE teams: work in progress.





T2.4 (MBN-RC, INFN, Uni-Mainz, UNIFE, HMU)

- **Theoretical and computational *characterisation of radiation emitted in CLSs*** based on different (i) manufactured crystal structures, (ii) propagation regimes, (iii) beam parameters.
- **Comparative characterisation/description and computational design of novel CLSs** which can be tuned for the beams available at existing and future facilities.

Definition of the term “CLS prototype”



CLS Prototype implies full characterization (experimental or/and theoretical and computational) of radiation emitted by a beam of charged projectiles passing through a crystalline target. The following data / parameters are to be specified / calculated / measured:

- 1) Data on the radiation emitted: spectral-angular and spectral distributions, photon flux (i.e. number of photons per second for given aperture), brilliance;
- 2) Parameters of the beam: type of the particles (electrons or positrons), beam energy, divergence, size, emittance, energy spread;
- 3) Data on the crystal target: type of the crystal, orientation, geometry (linear, bent, periodically bent), bending parameters (curvature radius, amplitude and period), thickness, crystal quality (defects concentration, bending homogeneity).

The quantities 1) and 2) are commonly used for the characterisation of other types of gamma-ray light sources (synchrotrons, Compton LS).

CLS to be compared to modern Compton gamma-ray LS

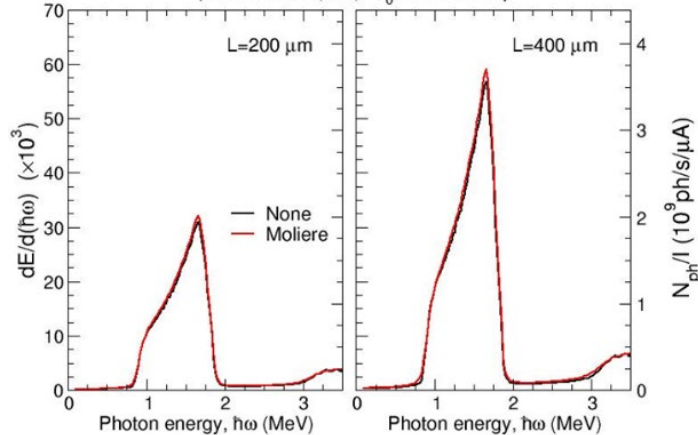
Parameters of several Compton gamma-ray light sources which are either operational or being developed for operation. Listed are: electron beam energy ε , average current I , gamma photons

Facility Location	HIGS (US)	LEPS/LEPS2 Japan	NewSUBARU Japan	UVSOR-III Japan	SLEGS China	ELI-NP Romania
ε (GeV)	0.24-1.2	8	0.5-1.5	0.75	3.5	0.23-0.74
I (mA)	10-120	100	300	300	100-300	1
$\hbar\omega$ (MeV)	1-100	1300-2900	1-40	1-5.4	0.4-20	1-19.5
$\Delta\omega/\omega$ (%)	0.8-10	<15	10	2.9	<5	<0.5
$(N_{\text{ph}})_{\text{tot}}$ (ph/s)	10^6 - 3×10^{10}	10^6 - 10^7	$(1-4) \times 10^7$	10^7	10^6 - 10^8	10^{11}

Theoretical & computational characterization of CLS Prototypes

(I) 500 MeV positrons and 855 MeV electrons in single diamond crystals

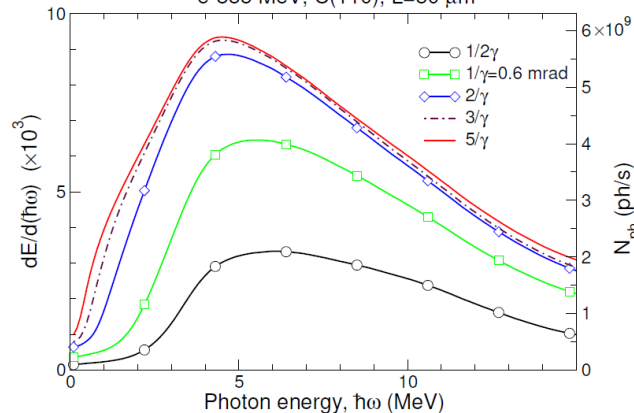
p-500 MeV, C(110), $\theta_0=1 \text{ mrad} = 1/\gamma$



MBN-RC: work in progress.

Spectral distribution of radiation (left axes) and number of photons per second and **per 1 μA** of the beam current (right axes) emitted by **500 MeV positrons** incident along the (110) planar direction in a 200 μm (left figure) and 400 μm (right figure) thick diamond crystals. The emission cone equals to the natural emission cone $1/\gamma = 1 \text{ mrad}$. The dependences have been calculated without (“None”) and with (“Moliere”) account for the ionizing collisions. The number of photons is calculated for the bandwidth $\Delta\omega/\omega = 0.01$.

e-855 MeV, C(110), L=50 μm

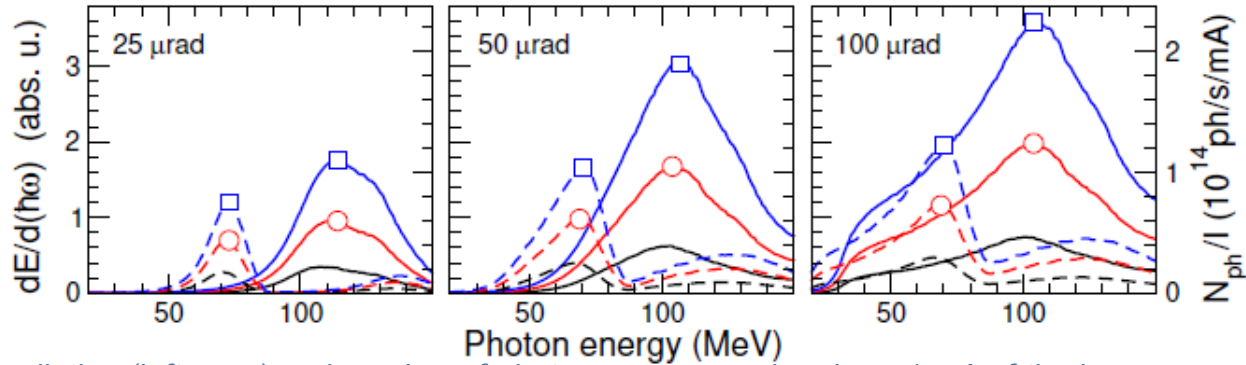


Spectral distribution of radiation (left axes) and number of photons per second and **per 1 μA** of the beam current (right axes) emitted by **500 MeV electrons** incident along the (110) planar direction in a 200 μm (left figure) and 400 μm (right figure) thick diamond crystals. The emission cone equals to the natural emission cone $1/\gamma = 1 \text{ mrad}$. The dependences have been calculated without (“None”) and with (“Moliere”) account for the ionizing collisions. The number of photons is calculated for the bandwidth $\Delta\omega/\omega = 0.01$.

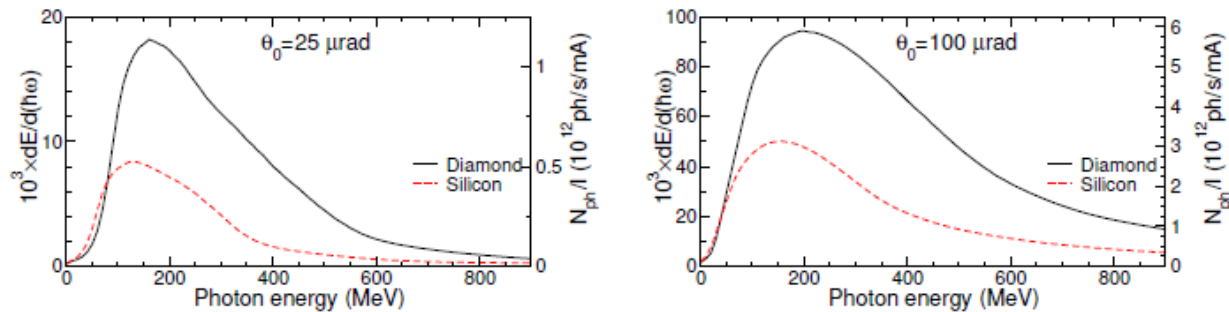
Work in progress (MBN-RC): CLS prototypes by means of single diamond crystals are feasible at MAMI energies for both electrons and positrons. **The intensity in the photon energy range 0.5-5 MeV can be up to 10^9 photons/s/ μA** thus making the CLS competitors to the existing gamma-ray LS based on the Compton scattering.

Theoretical & computational characterization of CLS Prototypes

(II) 10 GeV positrons and electrons in 0.1-6 mm single Si and Diamond crystals



Spectral distribution of radiation (left axes) and number of photons per second and per 1 mA of the beam current (right axes) emitted by **10 GeV positrons** incident along the (110) planar direction in diamond (solid lines) and silicon (dashed lines) crystals. The curves without symbols, with open circles and with open squares correspond to the crystal thickness 1, 3, and 6 mm, respectively. Three graphs refer to different emission cones as indicated. The number of photons is calculated for the bandwidth $\Delta\omega/\omega = 0.01$.



Spectral distribution of radiation (left vertical axes) and number of photons per second and per unit current in mA (right vertical axes) calculated for **10 GeV electrons** passing through 0.2 mm thick diamond and silicon crystals along the (110) planar direction. Left and right graphs correspond to the emission cones 25 and 100 μrad . The number of photons refers to the bandwidth $\Delta\omega/\omega = 0.01$.

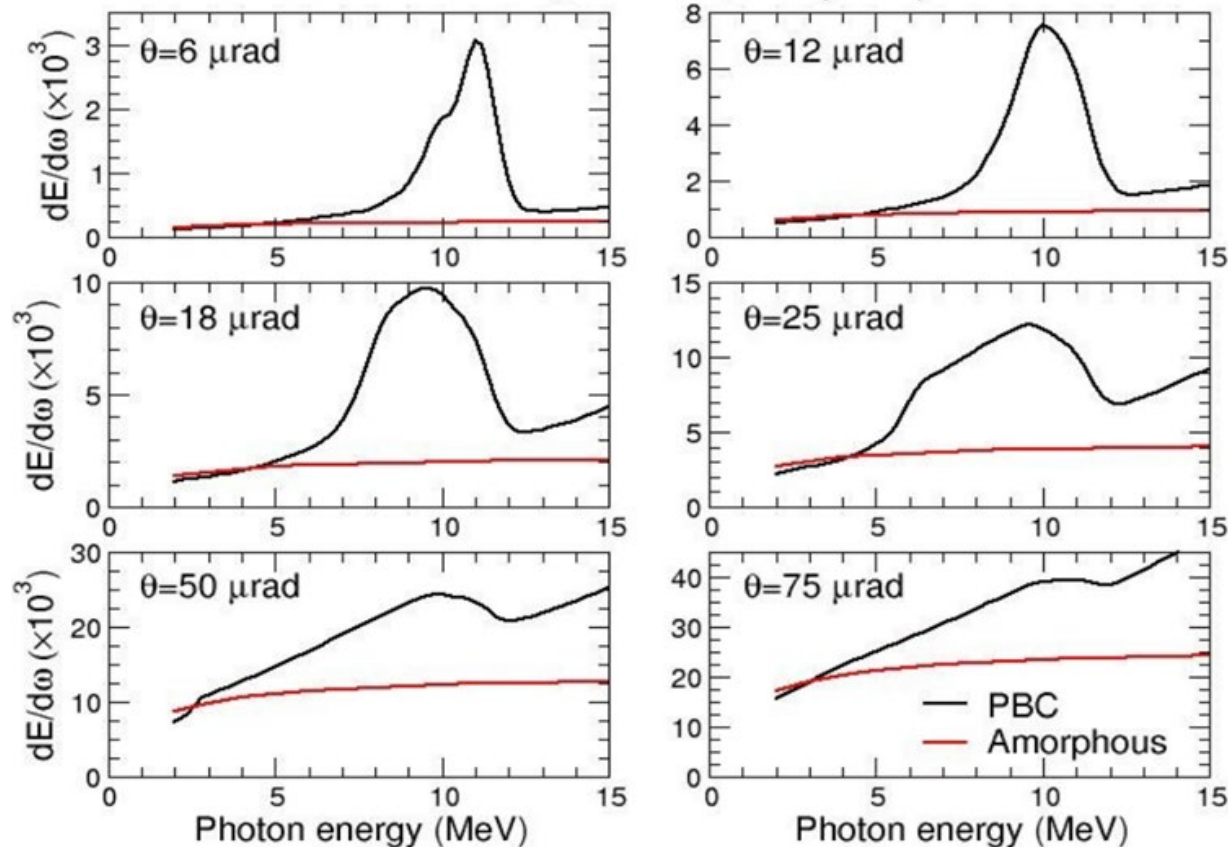
Summary: By means of CLS based on single crystals it is possible to achieve average photon fluxes much higher than those available at modern laser-Compton gamma-ray light sources.

G.B. Sushko, A.V. Korol, A.V. Solov'yov, arXiv:2401.10596 (24 Jan 2024).

Theoretical & computational characterization of CLS Prototypes



(III) 20 GeV positrons in acoustically excited Silicon crystals

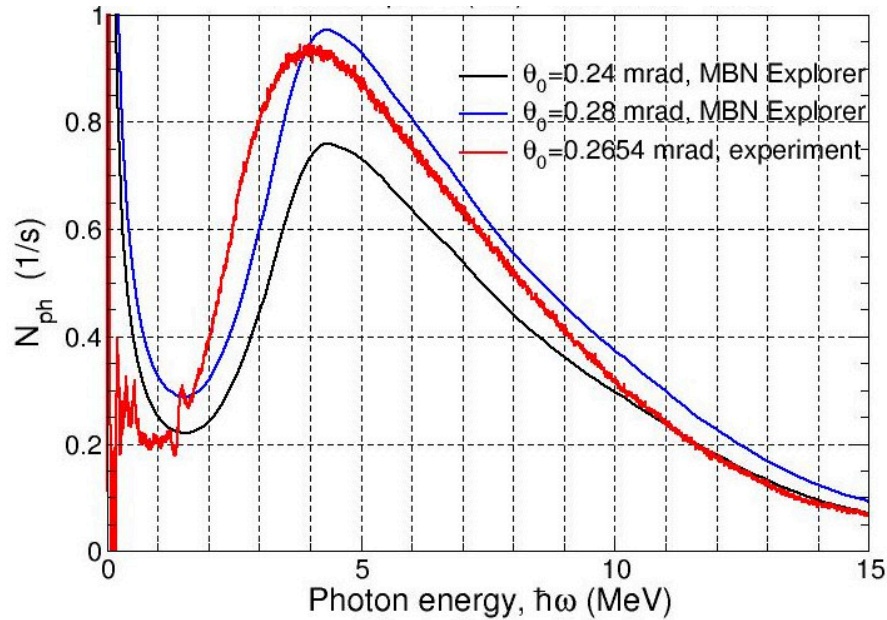


Spectral distribution of CUR (black curves) emitted by 20 GeV positrons in the acoustically excited silicon (110) crystal. Red curves show the distributions in amorphous silicon. Different graphs refer to different emission cones θ as indicated. The data corresponds to the AW frequency of 40 MHz..

Work in progress: MBN-RC & HMU.

Full characterization of the CLS prototype

855 MeV electrons in a diamond single crystal



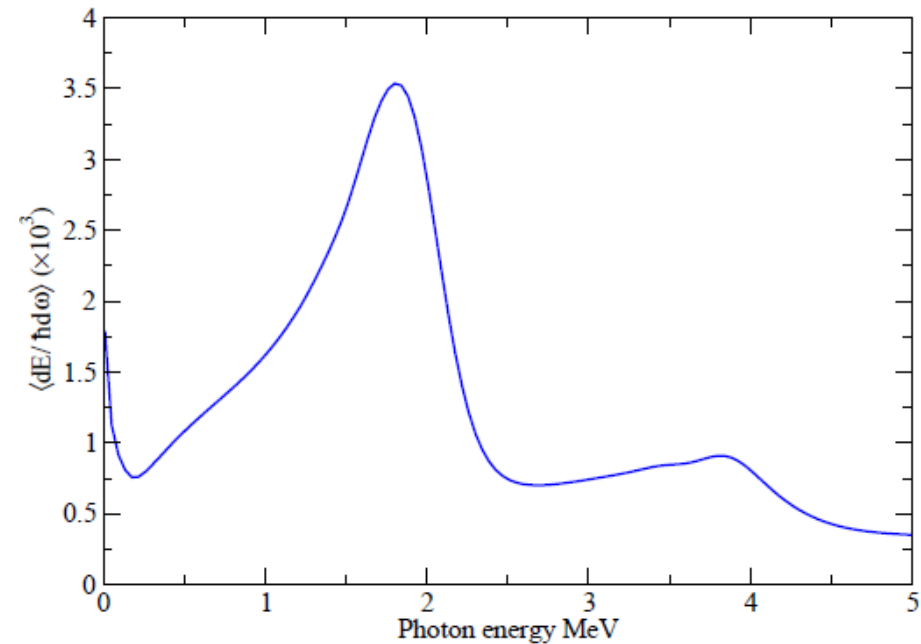
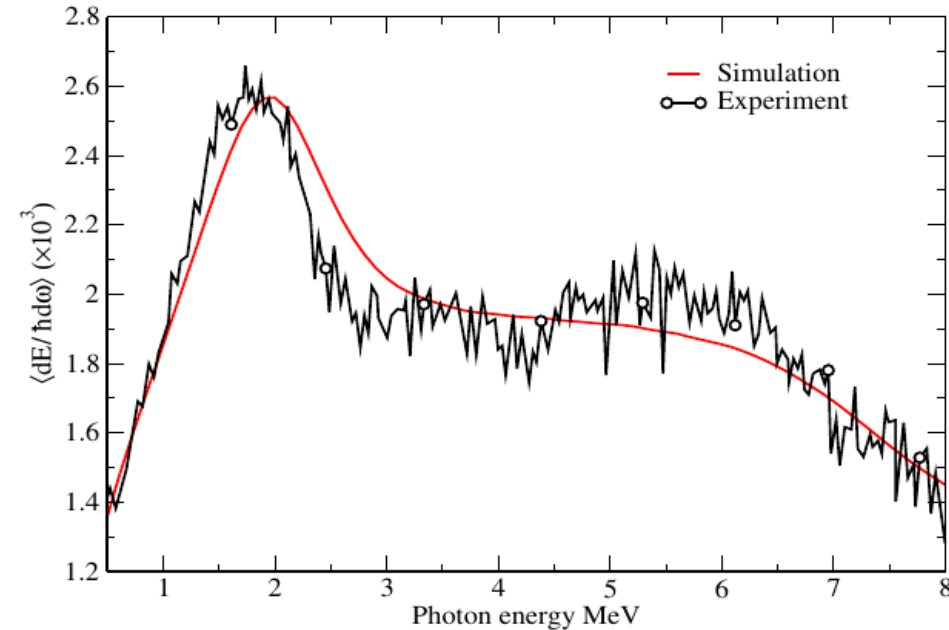
Number of photons (per second) emitted by 855 MeV and $I=0.166$ pA electron beam incident on a 50 microns thick diamond single crystal. In the experiment (Uni-Mainz) the photons were collected within the 0.2654 mrad cone along the incident beam direction. The simulations (MBN-RC) refer to the emission cones as indicated in the legend.

Note that the data on N_{ph} refer to low beam current I and to narrow bandwidth. Increasing the current up to 10 μ A (which is achievable at MAMI) and bandwidth by a factor of 25 (this will correspond to $\Delta\omega/\omega=0.01$ in the maximum at $\hbar\omega\approx 4$ MeV) the number of photons can be as high as 10^9 ph/s, thus exceeding N_{ph} achievable at many currently operating Compton gamma-ray LS.

Summary: We consider this result as full characterisation of the particular CLS based on the electron beam propagation through a single crystal. This is an important achievement of the Consortium work during the second year of the project.

Work in progress: MBN-RC & Uni-Mainz.

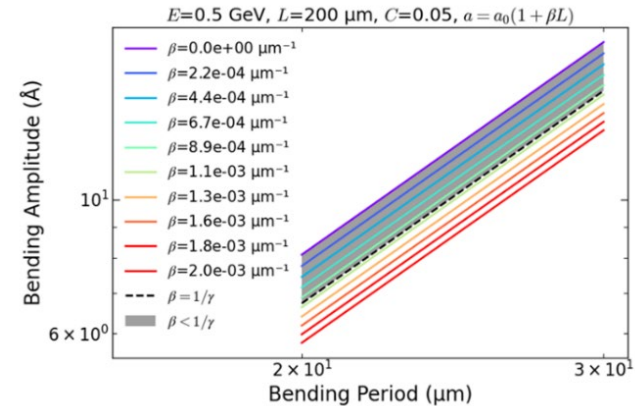
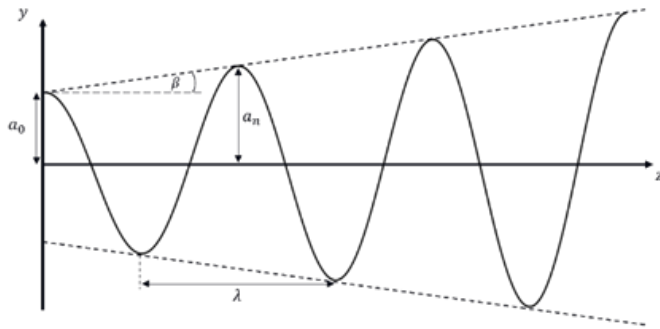
Radiation emission by 855 MeV e^-/e^+ in quasi-mosaic bent Si crystal



Spectral distribution of radiation emitted by 855 MeV electrons (left) and positrons (right) passing through the 'quasi-mosaic' bent Si(111) crystal. Solid (red and blue) curves without symbols stands for the results of the current simulations; solid (black) curve with symbols, shown in the left figure, corresponds to the experimental data reported by Bandiera et al *Phys. Rev. Lett.* 115 (2015) 025504. Note that the values of $\langle dE/d\hbar\omega \rangle$ are shown being multiplied by the factor 10^3 . The intensity of the of background radiation due to the incoherent bremsstrahlung is approximately 0.35×10^{-3} .

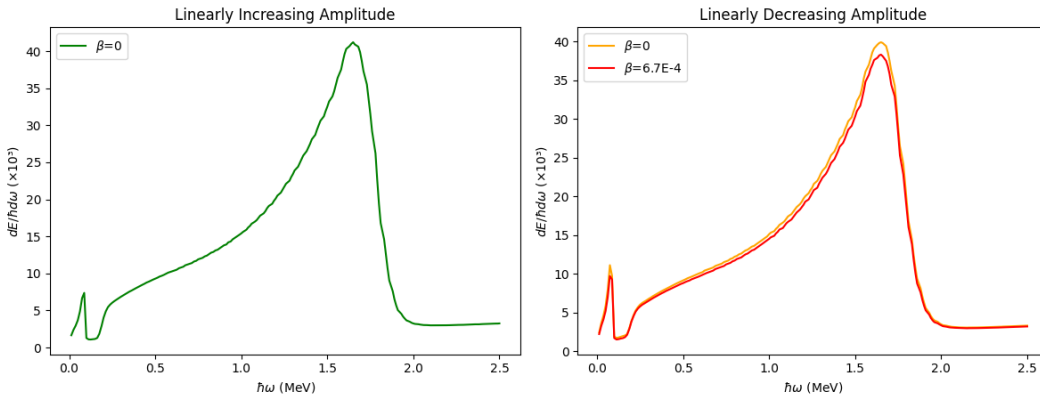
P.E Ibanez-Almaguer, G. Rojas-Lorenzo, M. Marquez-Mijares, J. Rubayo-Soneira, G.B. Sushko, A.V. Korol, A.V. Solov'yov, arXiv:2312.09927 (<https://arxiv.org/abs/2312.09927>) (15 Dec 2023).

Computational analysis of radiation emitted by projectiles moving along non-harmonic trajectories



Left: Schematic representation of the linearly increasing bending amplitude where β is the amplitude angle, a_0 is the initial amplitude and λ is the period. **Right:** Graphical aid for choosing the values of β ; Specific scenario considered, with the parameters shown in the figure title. One should aim for the values marked in grey to maintain the coherence of radiation.

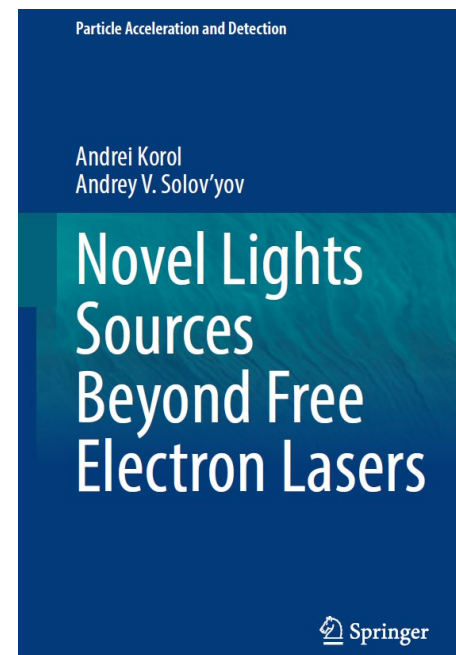
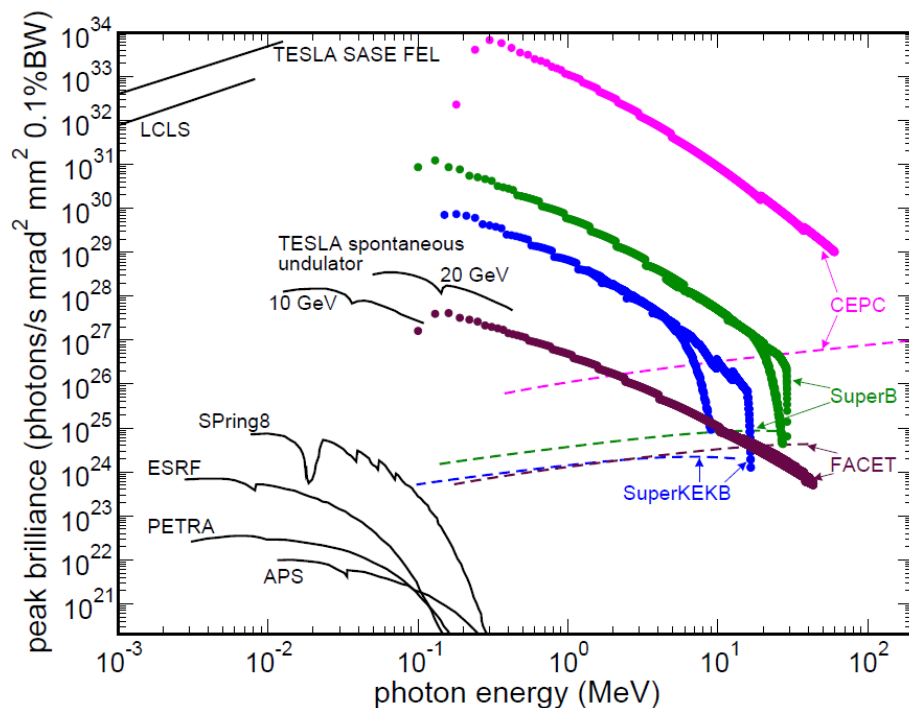
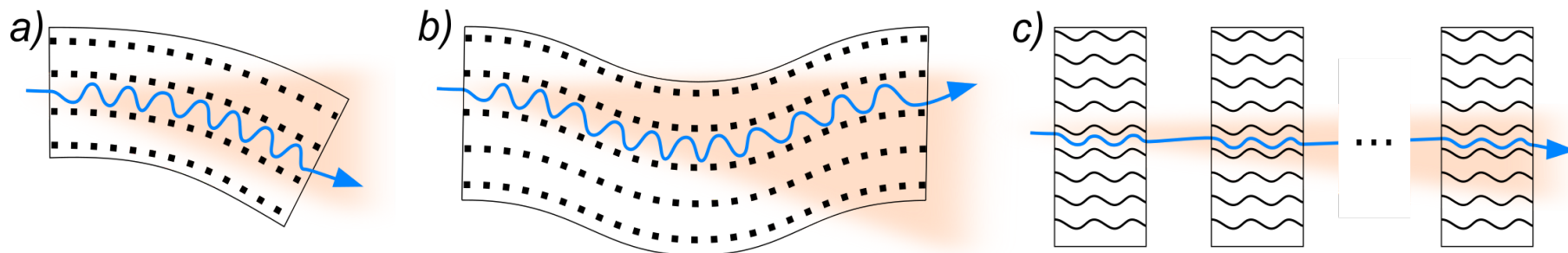
Spectral distribution of radiation emitted



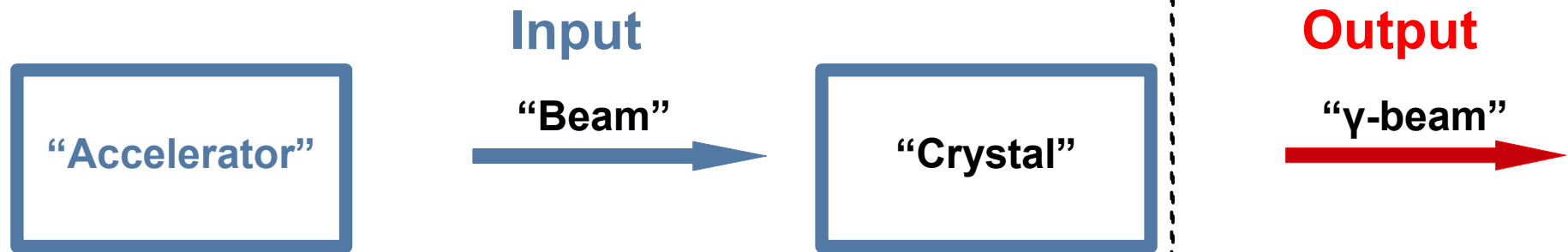
Spectral distribution of radiation emitted by positron channeling in periodically bent diamond (110) crystal with varied bending amplitude. Each plot presents the spectrum for a harmonic bending profile ($\beta = 0$) as well as non-harmonic profile; The initial values for bending amplitude are 11.2 Å (left) and 14.6 Å (right).

Work in progress: UoK & MBN-RC.

Conclusions and outlook



Realisation of the prototypes of gamma-ray Crystal-based LS (CLS)



Principal elements:

- Type of accelerator
- Apparatus
- Beam line

- Infrastructure

Characterisation of the beam:

- Type of projectile
- Energy and energy spread
- Size
- Emittance
- Current

Relevant issues:

- Crystal manufacture;
- Structure characterisation
- Crystal manipulation
- Channeling experiments
- Advanced simulations

Work in progress:
MBN-RC & TIMU.

Experimental and theoretical characterisation of the radiation:

- Spectral-angular distribution
- Number of photons
- Brilliance
- Power

MBN-RC & TECHNO-CLS consortium: TECHNO-CLS report

Table 4.5.2 List of suitable accelerator facilities TECHNO-CLS consortium: TECHNO-CLS report

Facility	Beam line	proj ctile	Beam parameters							Availa bility
			energy (GeV)	size (μm)	divergence (μrad)	repetition rate (pulse/s)	charge (units of e)	current peak ave	Already used	
MAMI		e ⁻	0.270- 0.855	x:10-1000 y:10-1000	x:100-1 y:800-8	CW [1]		0.16fA- 50 μ A (average)	Yes	A
MAMI		e ⁺	0.530	x:250 μm [2] y:1500 μm	x: [3] y: 60	CW [1]		1.6 fA (peak)	Yes	A
CERN	SPS-H2	e ⁻ , e ⁺	20- 120	x,y:(2-3)mm @120GeV	x:(325-90) @ (20-120) GeV; y:(230-100) @(20-120)GeV		10 ⁴ -10 ⁵ per spill [4]		YES, but parameters can be modified	yes
CERN	PS-T9	e ⁻	1-15	x,y: few cm	x:800@6GeV; y:1500@6GeV		10 ² -10 ³ per spill [5]		YES, but parameters can be modified	yes
CERN	PS-T9	e ⁺	1-15	x,y: few cm	x:800@6GeV; y:1500@6GeV		10 ² per spill [5]		YES, but parameters can be modified	yes

■ ■ ■ see report

Table 4.5.3 Conducted and planned experiments at synchrotrons and accelerators

a) Experiments conducted at synchrotrons and accelerators during the 1st year of the project

■ ■ ■ see report [TECHNO-CLS consortium: TECHNO-CLS report](#)

b) Experiments conducted at synchrotrons and accelerators during the 2nd year of the project

Facility	Beam line	Projectile	energy	Target	Data to be measured	Time	Teams
CERN	T9	e-/e+	6 GrV	Tungsten and Iridium single crystals	Radiative energy loss, photon yield	August 2023	INFN, UNIFE, UNIPD
MAMI	X1	e+	530 MeV	Si flat, Bent Si	Beam line tests, Channeling of Positrons, Deflection of Positrons	Several beam times 2023 - 2024	Uni Mainz, UNIFE, INFN, UNIPD
MAMI	X1	e-	600MeV -	Diamond,	Radiation Spectra,	Several beam	Uni Mainz, ESRF,

■ ■ ■ see report [TECHNO-CLS consortium: TECHNO-CLS report](#)

c) Schedule of planned experiments at synchrotrons and accelerators

Facility	Beam line	Projectile	energy	Target	Data to be measured	Time	Teams
MAMI	X1	e+	530 MeV	Flat Si, PBC SiGe,	Beam line tests, Channeling of	Several beam times 2024 -	Uni Mainz, UNIFE, INFN, UNIPD,

■ ■ ■ see report [TECHNO-CLS consortium: TECHNO-CLS report](#)

Types of crystals: material, geometry & technologies for crystal manufacturing



Table 4.5.1 Cumulative list of available crystals and related manufacturing technologies.

Silicon (Si)										
Label	Type	Method	Direction	Parameters [1]				Characteri- sation	Where stored	Availability (A, N/A)
				Size	R (cm)	a (nm)	λ (μm)			
BC-Si-QM1	BC	QM	(111)	L:15 μm	3	-	-	[2]	INFN, UNIFE	A
BC-Si-QM0	BC	QM	(111)	L:30 μm	3	-	-	[3]	INFN, UNIFE	A
BC-Si-St	BC	Si ₃ N ₄	(110)	L=4mm, W=55mm, T=0.5mm	8000	-	-	-	INFN, UNIFE	A
	PBC	Gr	(111)	L:0.8mm, W:2mm, T:200 μm , UndT:100 μm	-	0.15	80	[4]	INFN, UNIFE	A
PBC-Si-G1	PBC	Gr	(111)	L:3.2mm, W:10mm, T:200 μm ; UndT:160 μm	-	1.28	320	[4], [5]	INFN, UNIFE	A
	PBC	Si ₃ N ₄	(110)	L=10 λ T=160 μm , W to be defined depending on coating homogeneity. Range is to be selected depending on available facility	-	>1 Dep. on FEM simula- tion	350 500 1000		To be built at INFN, UNIFE	N/A [9]

■ ■ ■

see report

TECHNO-CLS consortium: TECHNO-CLS report

MBN Research Center (www.mbnresearch.com)

Table 4.5.4 List of CLS prototypes (theory, experiment, both) and related manufacturing technologies

Linear Crystals						
projectile	Beam	Material	Size	Type/ Technology	CLS	
					Spectrum	CLS characteristics
Diamond						
e	E=10 GeV $\sigma_x=6.8 \mu\text{m}$ $\sigma_y=16.3 \mu\text{m}$ $\gamma\epsilon_x=4.0\mu\text{m-rad}$ $\gamma\epsilon_y=3.2\mu\text{m-rad}$ $I_{\text{peak}}=6.4 \text{ kA}$	C(110)	L=6-96 μm		PhE=0.1-2 GeV SAD, SD – yes	PhNo – yes B_{peak} - yes
Ref. [1]	Ref. [1]	Ref. [1]	Ref. [1]		Ref. [1]	Ref. [1]
e	E=10 GeV $\sigma_{x,y}=6.8 \text{ \& } 16.3 \mu\text{m}$ $\gamma\epsilon_x=4.0\mu\text{m-rad}$ $\gamma\epsilon_y=3.2\mu\text{m-rad}$ $I = 1 \text{ mA}$	C(110)	L=200-400 μm	LC	PhE=50-600 MeV SAD, SD – yes	PhNo – yes B – yes
Ref. [2]	Ref. [2]	Ref. [2]	Ref. [2]		Ref. [2]	Ref. [2]
e+	E=10 GeV $\sigma_{x,y}=6.8 \text{ \& } 16.3 \mu\text{m}$ $\gamma\epsilon_x=4.0\mu\text{m-rad}$	C(110)	L=1000-6000 μm	LC	PhE=50-150 MeV SAD, SD – yes	PhNo – yes B – yes

■ ■ ■

see report TECHNO-CLS consortium: TECHNO-CLS report

Acknowledgement to the MBN RC team and the TECHNO-CLS Consortium



MBN
Research Center



MBN
Research Center



Istituto Nazionale di Fisica Nucleare

JOHANNES GUTENBERG
UNIVERSITÄT MAINZ



University of
Kent



UNIVERSITÀ
DEGLI STUDI
DI FERRARA
- EX LABORE FRUCTUS -



UNIVERSITÀ
DEGLI STUDI
DI PADOVA

Thank you for your attention !